Confluence of geodesic paths and separating loops in large planar quadrangulations

J. Stat. Mech. (2009) P03001

(http://iopscience.iop.org/1742-5468/2009/03/P03001)

Journal of Statistical Mechanics: Theory and Experiment
An IOP and SISSA journal

Confluence of geodesic paths and separating loops in large planar quadrangulations

J Bouttier and E Guitter

Institut de Physique Théorique, CEA, IPhT, F-91191 Gif-sur-Yvette, France
and
CNRS, URA 2306, F-91191 Gif-sur-Yvette, France
E-mail: jeremie.bouttier@cea.fr and emmanuel.guitter@cea.fr

Received 6 November 2008
Accepted 28 January 2009
Published 2 March 2009

Online at stacks.iop.org/JSTAT/2009/P03001
doi:10.1088/1742-5468/2009/03/P03001

Abstract. We consider planar quadrangulations with three marked vertices and discuss the geometry of triangles made of three geodesic paths joining them. We also study the geometry of minimal separating loops, i.e. paths of minimal length among all closed paths passing by one of the three vertices and separating the two others in the quadrangulation. We concentrate on the universal scaling limit of large quadrangulations, also known as the Brownian map, where pairs of geodesic paths or minimal separating loops have common parts of non-zero macroscopic length. This is the phenomenon of confluence, which distinguishes the geometry of random quadrangulations from that of smooth surfaces. We characterize the universal probability distribution for the lengths of these common parts.

Keywords: rigorous results in statistical mechanics, correlation functions (theory), exact results, random graphs, networks

ArXiv ePrint: 0811.0509

1742-5468/09/P03001+44$30.00

Contents

1. Introduction

Understanding the geometry of large random quadrangulations is a fundamental issue relating combinatorics, probability theory and statistical physics. Indeed random quadrangulations, or more generally random maps, provide natural discrete models for random surfaces, for instance in the context of two-dimensional quantum gravity [1]–[3], and may mathematically be viewed as metric spaces endowed with the graph distance. In the same way that discrete random walks converge to the Brownian motion in a suitable scaling limit, random planar quadrangulations are expected to converge to the so-called Brownian map [4, 5] in the scaling limit where the size of the quadrangulation becomes large jointly with the fourth power of the scale at which distances are measured. This Brownian map is moreover expected to be the universal scaling limit for many models of planar maps such as random planar triangulations or more generally maps with arbitrary bounded face degrees or even maps coupled to non-critical statistical models. It can be constructed as a random metric space and has been shown to be homeomorphic to the two-dimensional sphere [6, 7].

A number of local properties of the Brownian map can be derived from a detailed analysis of discrete maps. In this spirit, the simplest observable in the Brownian map is

J. Stat. Mech. (2009) P03001

the distance between two points. The statistics of this distance is characterized by the so-called two-point function and was obtained in [8] via scaling arguments for large triangulations, and in [9] via an exact computation of the discrete two-point function for planar quadrangulations. A related quantity is the radius, whose law was studied in [10, 11]. The question of estimating the number of geodesics (i.e. paths of shortest length) between two points was addressed later [12] and it was found that for typical points, all geodesics coalesce into a unique macroscopic geodesic path in the scaling limit [13, 14].

Properties involving three points on the map give a much richer geometric information. For instance, we may consider the 'triangle' made by the three geodesics between these points. In a previous paper [15], the authors have computed the joint probability distribution for the pairwise distances between three uniformly chosen random vertices in a random quadrangulation. In the scaling limit, this yields the so-called three-point function of the Brownian map, which can interpreted as the joint law for the three side lengths of the triangle. The three-point function was considered previously in [16] where an expression involving two distances only was obtained and used as a basis for an operator product expansion analysis in the limit where two of the points approach each other. The full dependence on the three distances was found in [15] as a corollary of the exact discrete expression for quadrangulations. On the other hand, it was recognized by Le Gall that geodesics exhibit a phenomenon of *confluence* [14]. In our setting, this means that any two sides of the triangle merge before reaching their common end-point, and hence have a common part of non-zero macroscopic length. This is quite unlike the case for smooth surfaces where two sides of a triangle only meet at their end-point. Thus a full characterization of the geometry of triangles involves six lengths, which are those of the three segments proper to each side and of the three segments common to two sides (see figure 1(a)), as well as two areas for the two domains in the map delimited by the triangle.

Beyond triangles, another interesting geometric construction involving three points is what we call a minimal separating loop, defined as follows: given three distinguished points, say v_1, v_2 and v_3, we define a separating loop as a closed path passing through v_3 and *separating* v_1 *from* v_2, in the sense that any path from v_1 to v_2 necessarily intersects it. A minimal separating loop is such a separating loop with minimal length. We expect the minimal separating loop to be unique at a macroscopic level, and to have a finite macroscopic length (note that, if we relax the condition that the loop passes through v_3 or that it separates v_1 from v_2, then clearly we can find loops of arbitrarily small length). Moreover, its two halves are geodesic paths and we again expect a phenomenon of confluence, namely the two halves share a macroscopic common segment (see figure 1(b)). The characterization of the geometry of minimal separating loops involves therefore the lengths of its common and 'open' parts, as well as the areas of the two domains delimited by the loop.

In this paper, we derive the probability distributions for the above parameters characterizing triangles and loops when the three points are chosen uniformly at random. This is done by explicit computations of the discrete counterparts of these distributions in the framework of planar quadrangulations, using the methodology developed in [15] and based on the Schaeffer [17] and Miermont [13] bijections between quadrangulations and well-labeled maps.

The paper is organized as follows. In section 2, we give a precise definition of minimal separating loops in triply pointed planar quadrangulations and compute the generating

J. Stat. Mech. (2009) P03001

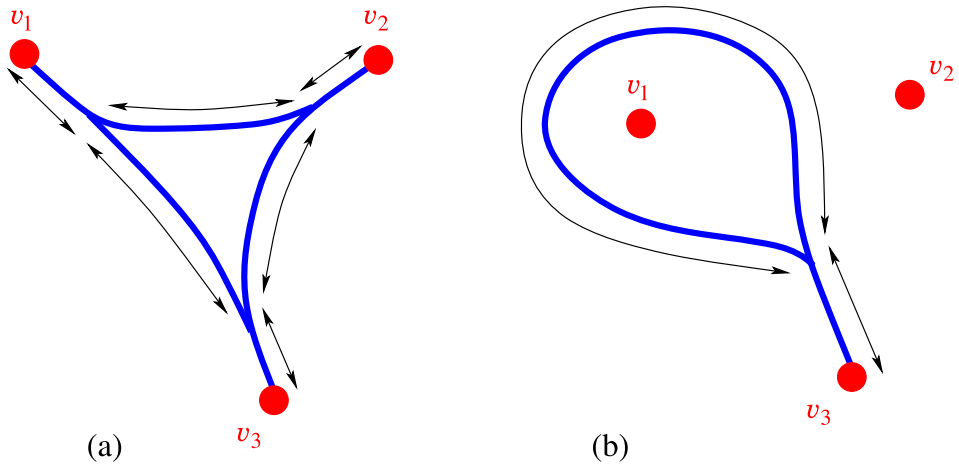

Figure 1. A schematic picture of the phenomenon of confluence for the geometry of triangles (a) and separating loops (b) in the scaling limit of large maps. In (a), the three geodesics (represented as thick blue lines) linking the three points v_1, v_2 and v_3 have common parts of macroscopic length. The triangle is therefore characterized by six lengths (as indicated by double arrows) and by the area of the two domains delimited by its open part. In (b), a minimal separating loop passing by v_3 and separating v_1 from v_2 also has a common part of macroscopic length and is therefore characterized by two lengths (as indicated by double arrows) and by the area of the two domains delimited by its open part.

function for such quadrangulations with a *prescribed value for the loop length*. To this end, we provide in section 2.1 two alternative bijections based on the Schaeffer and Miermont constructions relating the desired class of triply pointed quadrangulations with suitable classes of well-labeled trees or maps. In section 2.2, we calculate their generating functions by expressing them in terms of basic building blocks already computed in [15]. Section 2.3 is devoted to the analysis of the scaling limit, with a particular emphasis on the universal probability law for the length of the minimal separating loop, as well as its correlation with the distances between the marked vertices. In section 3, we turn to the phenomenon of confluence, which we analyze via a refinement of the above enumeration. In section 3.1, we give the probability law for the length of the part common to two geodesics leading to the same vertex. We then investigate the phenomenon of confluence for minimal separating loops in section 3.2 where we derive the probability distribution for the parameters characterizing the geometry of these loops. Section 4 is devoted to the geometry of triangles. There we revisit the bijection of [15] and solve a refined enumeration problem in order to keep track of the six lengths characterizing the triangle. We deduce their joint law in the scaling limit, and provide explicit expressions for a number of marginal laws. We discuss our results and conclude in section 5.

2. Minimal separating loops

Consider a quadrangulation of the sphere, i.e. a planar map whose faces all have degree 4, equipped with three marked distinct vertices v_1, v_2 and v_3. As is customary for

J. Stat. Mech. (2009) P03001

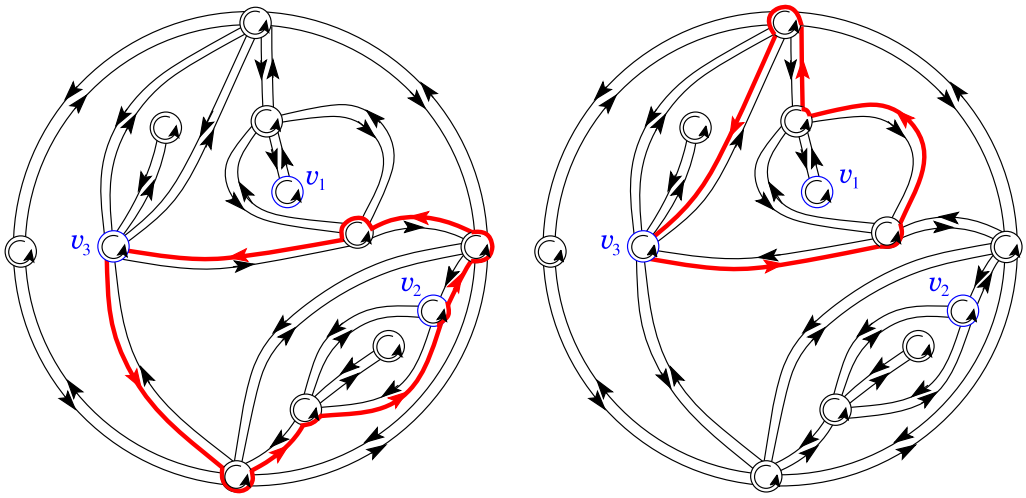

Figure 2. A quadrangulation with three marked vertices v_1, v_2 and v_3, represented as a traffic network, i.e. a ribbon graph with roundabouts. In (a), we show (red thick lines) a particular separating loop of length 6. In (b), the indicated separating loop is minimal, i.e. has a minimal length (here 4) among the loops passing through v_3 and separating v_1 from v_2.

orientable maps, we may represent the map as a ribbon graph by splitting each edge of the quadrangulation into two oriented half-edges (with opposite orientations) so that half-edges are oriented clockwise around each face (see figure 2). It is also convenient to place a small counterclockwise oriented roundabout around each vertex so that the map looks like a traffic network. We can then consider (oriented) paths on this traffic network, and in particular loops made of a closed non-intersecting circuit starting from and returning back to the marked vertex v_3. Any such loop separates the sphere into two simply connected domains. Note that any vertex along the loop naturally belongs to exactly one of these domains, by following the roundabout convention. The circuit is called a *separating loop* if the marked vertices v_1 and v_2 do not lie in the same domain (see figure 2 for an illustration). The length of a circuit is the number of half-edges that it passes through. A *minimal separating loop* is a separating loop of minimal length.

Clearly the length l_{123} of a minimal separating loop is strictly positive and, from the bipartite nature of planar quadrangulations, it is even. Also, if we call d_{13} (respectively d_{23}) the graph distance from v_1 (respectively v_2) to v_3, following a geodesic path back and forth from v_3 to the closest vertex v_1 or v_2 forms a separating loop of length $2\min(d_{13}, d_{23})$, therefore:

$$l_{123} \leq 2\min(d_{13}, d_{23}). \tag{2.1}$$

The purpose of the following sections is to enumerate triply pointed quadrangulations whose three marked vertices have prescribed values of d_{13}, d_{23} and l_{123}.

An alternative definition of separating loops, mentioned in the introduction, consists in taking arbitrary (possibly self-intersecting) closed paths passing through v_3 and such that any path from v_1 to v_2 necessarily intersects them. This gives rise to a broader set of

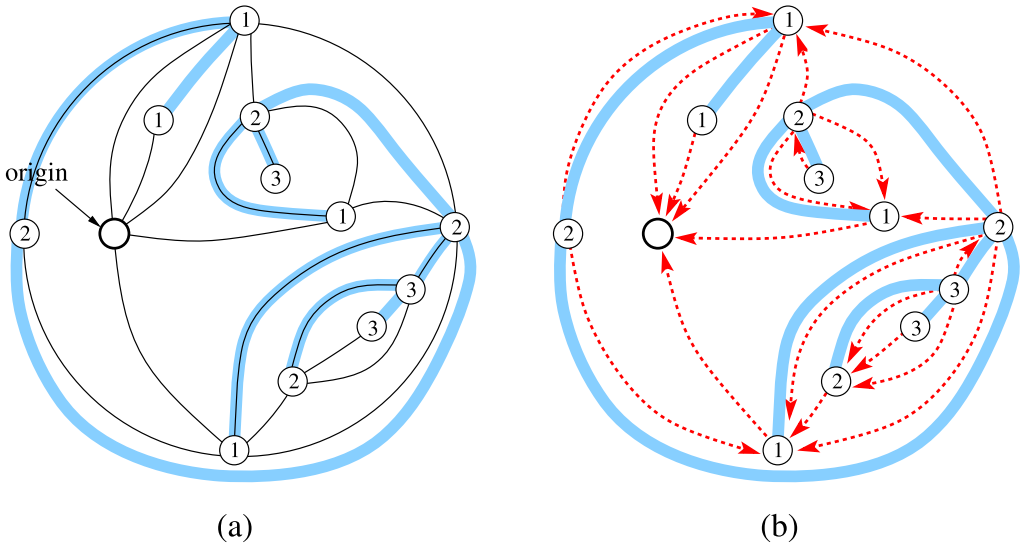

Figure 3. The quadrangulation of figure 2 with a marked origin (corresponding to v_3 in figure 2) and its coding (a) by a well-labeled tree (blue thick lines). The quadrangulation is recovered from the well-labeled tree by connecting each corner to its successor (dashed red arrows in (b)).

minimal separating loops but does not affect the minimal length since any such minimal separating loop can be transformed into a non-self-intersecting circuit of the same length by 'undoing' the crossings.

2.1. Combinatorics

2.1.1. Approach via the Schaeffer bijection. It is well-known [18] that any planar quadrangulation with n faces and a marked origin vertex is in one-to-one correspondence with a *well-labeled tree* with n edges and with minimal label 1. Here we define a well-labeled tree as a plane tree with vertices carrying integer labels ℓ satisfying

$$|\ell(v) - \ell(v')| \leq 1 \qquad \text{if } v \text{ and } v' \text{ are adjacent in the tree.} \tag{2.2}$$

As shown by Schaeffer [17], this tree can be drawn directly on the quadrangulation by applying local rules which associate with each face of the quadrangulation an edge of the tree (see figure 3). The tree spans all vertices of the quadrangulation except the origin, and the label of each vertex is nothing but its graph distance to the origin in the quadrangulation. Conversely, to recover the quadrangulation from the well-labeled tree, we draw non-crossing arches connecting every *corner* of the tree to its *successor*. Recall that a corner is the sector between two consecutive edges around a vertex, and the successor of a corner with label $\ell > 1$ is the first corner with label $\ell - 1$ encountered after it clockwise along the contour of the tree, while all corners with label 1 have the same successor which is an extra vertex added in the external face (see figure 3(b)). The arches form the edges of the quadrangulation and the added vertex is the origin. Note that the *chain of successors* of a given corner (i.e. its successor, the successor of its successor, and

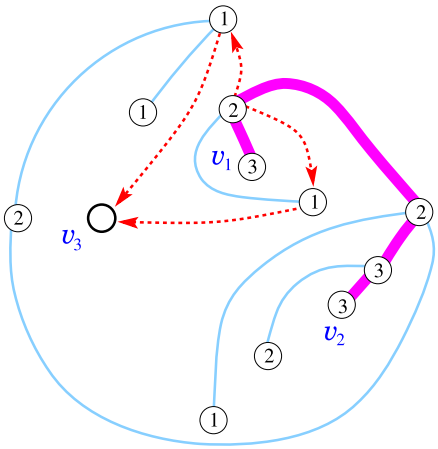

Figure 4. A well-labeled tree with two marked vertices v_1 and v_2. The edges of the branch from v_1 to v_2 are represented as magenta thick lines and the other edges as light-blue thin solid lines. The vertex v_3 is the origin added in the external face. We consider a vertex of minimal label (here 2) on the branch from v_1 to v_2 and represent the chains of successors (dashed red arrows) starting from two of its corners, one on each side of the branch. These form a minimal loop separating v_1 from v_2 and passing through v_3.

so on until the origin is reached) provides a geodesic path from the associated vertex to the origin.

In the case of a triply pointed quadrangulation, we can take v_3 as the origin vertex and we end up with a well-labeled tree with two marked vertices v_1 and v_2 carrying labels $\ell(v_1) = d_{13}$ and $\ell(v_2) = d_{23}$. Let us now explain how the quantity l_{123} can be read off the tree. Within the tree, there is a unique branch connecting v_1 to v_2 (see figure 4). Any loop separating v_1 from v_2 in the quadrangulation must intersect this branch at some vertex v. Decomposing the loop into a first part from v_3 to v and a second part from v back to v_3, both parts have length larger that the distance $\ell(v)$ from v to v_3, and we find that the length of the loop is larger than $2\ell(v)$, and hence larger than $2u$, where u is the minimal label encountered along the branch from v_1 to v_2. This holds in particular for minimal separating loops, and we therefore have $l_{123} \geq 2u$. Conversely, a separating loop of length $2u$ is obtained by considering a vertex with minimal label u on the branch, picking two corners on opposite sides of the branch and considering the chain of successors of these two corners which are both paths to v_3 of length u (see figure 4). This implies $l_{123} \leq 2u$ and therefore $l_{123} = 2u$. More generally, any minimal separating loop crosses the branch at a vertex with minimal label u, and hence it is made of two geodesic paths of the same length u joining the origin to that vertex which they reach from both sides of the branch.

For consistency with the alternative approach described below, we decide to shift all labels on the well-labeled tree by $-u$ so that the minimal label on the branch from v_1 to v_2 becomes 0. The minimal label in the whole tree is now $1 - u$, while v_1 and v_2 receive respective non-negative labels $s \equiv d_{13} - u$ and $t \equiv d_{23} - u$ (see figure 5 for an illustration). To conclude, triply pointed quadrangulations with prescribed values of d_{13}, d_{23} and l_{123} are in one-to-one correspondence with well-labeled trees having two marked vertices labeled

J. Stat. Mech. (2009) P03001

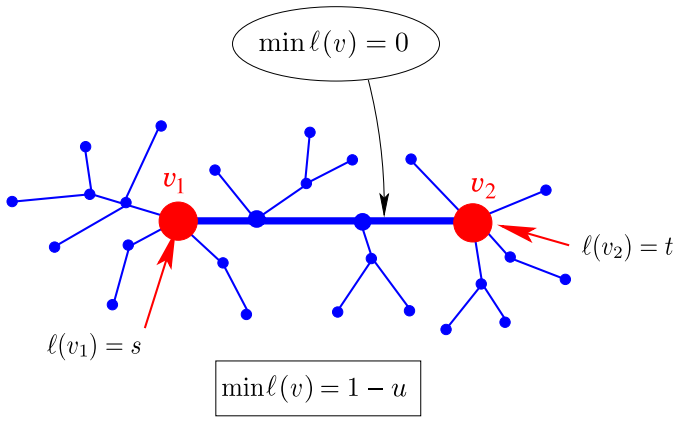

Figure 5. The well-labeled tree coding a triply pointed quadrangulation with prescribed values of d_{13}, d_{23} and l_{123}. It has two marked vertices v_1 and v_2 with respective labels $s = d_{13} - l_{123}/2$ and $t = d_{23} - l_{123}/2$. The minimal label on the branch between v_1 and v_2 is 0 and the global minimal label is $1 - u = 1 - l_{123}/2$.

$s = d_{13} - l_{123}/2$ and $t = d_{23} - l_{123}/2$, such that the minimal label on the branch joining these two vertices is 0 and the global minimal label in the tree is $1 - u = 1 - l_{123}/2$.

2.1.2. Approach via the Miermont bijection. An alternative approach is based on a bijection by Miermont [13] generalizing the Schaeffer bijection to multiply pointed planar quadrangulations. More precisely, the Miermont bijection acts on a quadrangulation equipped with, say p marked vertices $v_1, v_2, \ldots, v_p$ called *sources* and p integers $\tau_1, \tau_2, \ldots, \tau_p$ called *delays*, satisfying the conditions

$$\begin{aligned} &|\tau_i - \tau_j| < d_{ij}, \qquad 1 \leq i \neq j \leq p, \\ &\tau_i - \tau_j + d_{ij} \text{ is even}, \qquad 1 \leq i, j \leq p, \end{aligned} \tag{2.3}$$

where d_{ij} is the graph distance between v_i and v_j. It results in a planar map with p faces that is well-labeled, i.e. its vertices carry integer labels ℓ satisfying

$$|\ell(v) - \ell(v')| \leq 1 \qquad \text{if } v \text{ and } v' \text{ are adjacent in the map.} \tag{2.4}$$

Again, this map can be drawn directly on the quadrangulation by applying local rules which associate with each face of the quadrangulation an edge of the map (see figure 6). The map spans all vertices of the quadrangulation except the p sources and the label of a vertex v is given by

$$\ell(v) = \min_{j=1,\ldots,p} d(v, v_j) + \tau_j, \tag{2.5}$$

where $d(v, v_j)$ is the graph distance from v to the source v_j in the quadrangulation. Each face of the well-labeled map encloses exactly one source of the quadrangulation and we call the faces $f_1, f_2, \ldots, f_p$ accordingly. We furthermore have the property that, for any vertex v incident to f_i, the minimum in (2.5) is attained for $j = i$, i.e. $d(v, v_i) = \ell(v) - \tau_i$. In particular, the minimal label among vertices incident to f_i is $\tau_i + 1$, corresponding to nearest neighbors of v_i.

J. Stat. Mech. (2009) P03001

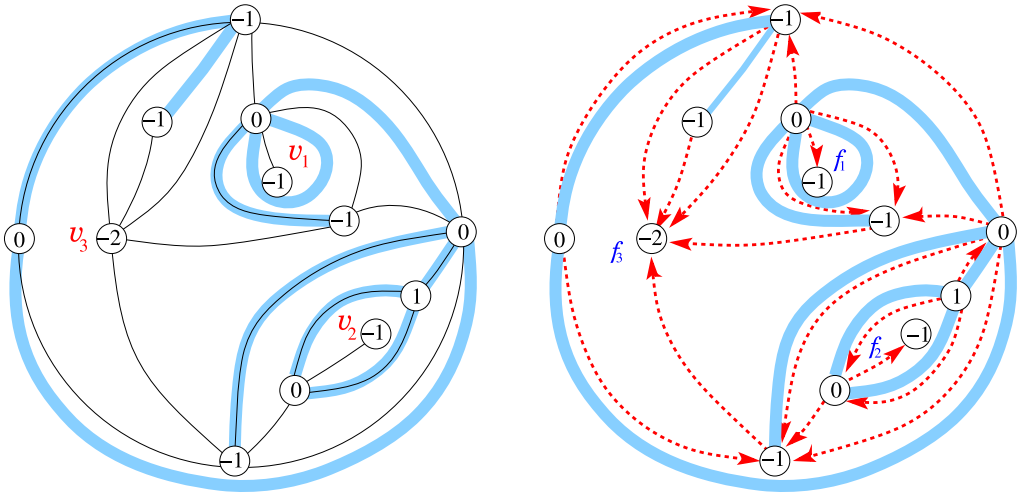

Figure 6. The quadrangulation of figure 2 with three marked vertices v_1, v_2, v_3, and its coding (a) by a well-labeled map (blue thick lines) using the Miermont bijection with particular delays $\tau_1 = \tau_2 = -1$ and $\tau_3 = -2$. The quadrangulation is recovered from the well-labeled map by connecting each corner to its successor (dashed red arrows in (b)).

Conversely, to recover the quadrangulation from the well-labeled map, we add inside each face f_i an extra vertex with label τ_i where

$$\tau_i = \min_{v \text{ incident to } f_i} \ell(v) - 1, \tag{2.6}$$

and each corner with label ℓ inside f_i is connected by an arch to its successor, which is the first corner with label $\ell - 1$ encountered counterclockwise inside the face (corresponding for the external face to the clockwise orientation around the map). The arches form the edges of the quadrangulation and the added vertices are the sources (see figure 6(b)).

Let us now see how to use the Miermont bijection to address the specific question of three marked vertices with prescribed values of d_{13}, d_{23} and l_{123}. As in [15], the idea is to supplement the Miermont bijection (here with $p = 3$ sources) with a particular choice of delays related to d_{13}, d_{23} and l_{123}. This particular choice will restrict the topology of the resulting well-labeled maps with three faces, and induce extra conditions on labels. More precisely, from the inequality (2.1), we may use the following parameterization:

$$d_{13} = s + u, \qquad d_{23} = t + u, \qquad l_{123} = 2u, \tag{2.7}$$

with s, t, u non-negative integers, and moreover $u \neq 0$. Our particular choice of delays is

$$\tau_1 = -s = l_{123}/2 - d_{13}, \qquad \tau_2 = -t = l_{123}/2 - d_{23}, \qquad \tau_3 = -u = -l_{123}/2. \tag{2.8}$$

Note that this particular choice fulfils the general condition (2.3) except when we have the equality $l_{123} = 2\min(d_{13}, d_{23})$, i.e. when s or t vanishes. This particular case must be treated separately, as will be explained below.

Assuming s and t strictly positive, a close look at the properties resulting from the choice of delays (2.8) in the Miermont bijection shows that the resulting well-labeled map

J. Stat. Mech. (2009) P03001

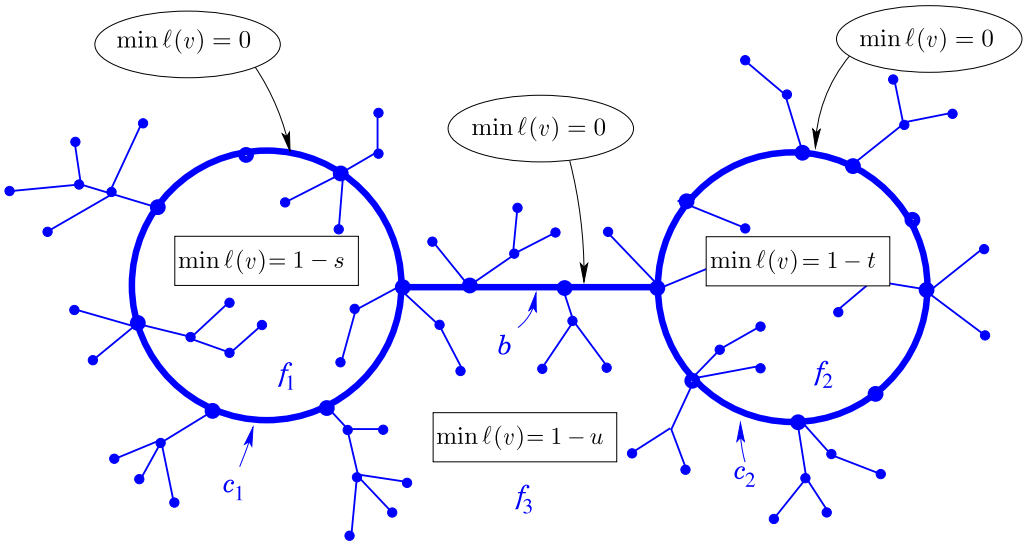

Figure 7. The well-labeled map with three faces coding a triply pointed quadrangulation with prescribed values of d_{13}, d_{23} and l_{123}, in the case $l_{123} < \min(d_{13}, d_{23})$. The faces f_1 and f_2 are not adjacent, and their frontiers with the face f_3 form two cycles c_1 and c_2, connected by a bridge b, whose edges are adjacent to f_3 only. The minimal label for vertices incident to f_1 (respectively f_2 and f_3) is $1 - s = 1 - d_{13} + l_{123}/2$ (respectively $1 - t = 1 - d_{23} + l_{123}/2$ and $1 - u = 1 - l_{123}/2$). The minimal label on the cycle c_1 is 0, as is that on the cycle c_2 and that on the bridge b.

is necessarily of the type displayed in figure 7. In particular, we find that any minimal separating loop must remain inside the face f_3; hence *the faces f_1 and f_2 cannot be adjacent*, i.e. cannot be incident to a common edge. The map can be viewed as made of a skeleton map (thick lines and big dots in figure 7) to which trees are attached. The skeleton is necessarily made of two *cycles* c_1 and c_2, which form respectively the frontier between f_1 and f_3, and that between f_2 and f_3, together with a *bridge* b connecting c_1 to c_2, and whose edges are only incident to f_3. Moreover, the labels must satisfy the following constraints (see figure 7):

$$\min_{\substack{v \text{ incident} \\ \text{to } f_1}} \ell(v) = 1 - s, \qquad \min_{\substack{v \text{ incident} \\ \text{to } f_2}} \ell(v) = 1 - t, \qquad \min_{\substack{v \text{ incident} \\ \text{to } f_3}} \ell(v) = 1 - u,$$
$$\min_{v \text{ on } c_1} \ell(v) = 0, \qquad \min_{v \text{ on } c_2} \ell(v) = 0, \qquad \min_{v \text{ on } b} \ell(v) = 0. \tag{2.9}$$

The first three constraints are general consequences of the Miermont bijection and rephrase the general condition (2.6), while the last three constraints result from our particular choice of delays, and can be obtained by arguments similar to those presented in [15]. More precisely, the constraint on c_1 (respectively c_2) ensures that the distance between v_1 and v_3 (respectively v_2 and v_3) is $s + u$ (respectively $t + u$), while the constraint on b ensures that the length of a minimal separating loop is $2u$. Note that the bridge b can be reduced to a single vertex, necessarily with label 0.

When $s = 0$ and $t > 0$, we apply the Miermont bijection with $p = 2$ sources only, namely v_2 and v_3, and delays $\tau_2 = -t$, $\tau_3 = -u$. We obtain a well-labeled map with two

J. Stat. Mech. (2009) P03001

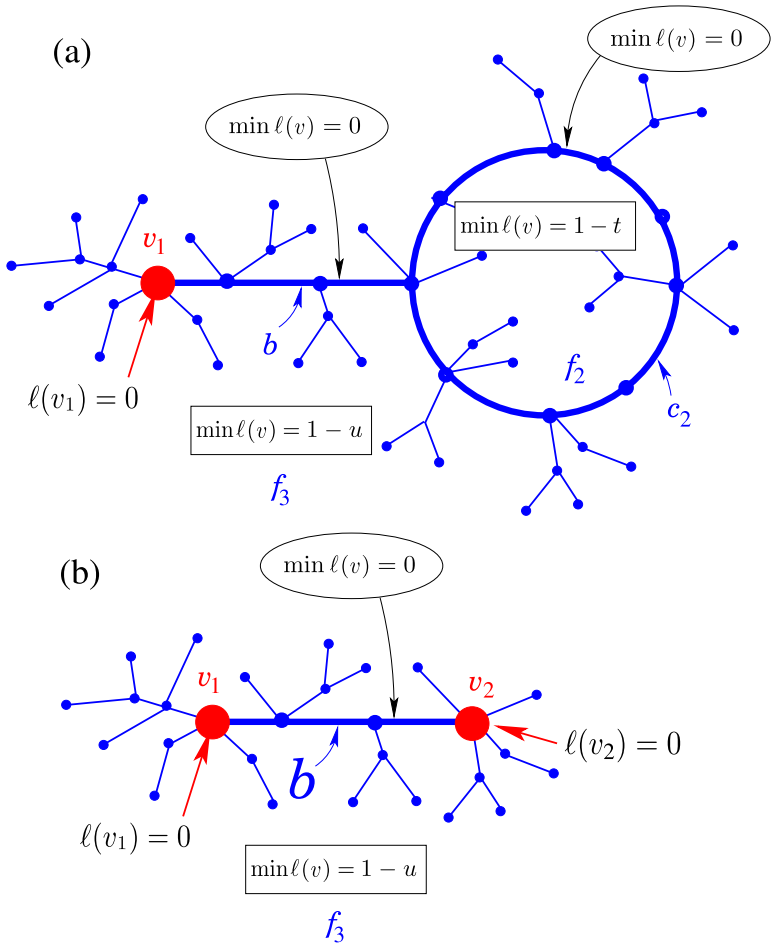

Figure 8. (a) The well-labeled map with two faces and a marked vertex coding a triply pointed quadrangulation with prescribed values of d_{13}, d_{23} and l_{123}, in the case $l_{123} = d_{13} < d_{23}$. The marked vertex v_1 is incident to the face f_3 and is connected to the frontier c_2 between f_2 and f_3 by a bridge b (whose edges are adjacent to f_3 only). The label of v_1 is 0 and the minimal label for vertices incident to f_2 (respectively f_3) is $1-t = 1-d_{23}+l_{123}/2$ (respectively $1-u = 1-l_{123}/2$). The minimal label on the cycle c_2 is 0, as is that on the bridge b. (b) The well-labeled tree with two marked vertices coding a triply pointed quadrangulation with prescribed values of d_{13}, d_{23} and l_{123}, in the case $l_{123} = d_{13} = d_{23}$. The marked vertices v_1 and v_2 are connected by a branch b and have label 0. The global minimal label is $1-u = 1-l_{123}/2$, while the minimal label on the branch b is 0.

faces of the type illustrated in figure 8(a). In particular, v_1 is necessarily incident to f_3 and has label 0, and is connected to the frontier between f_2 and f_3 by a bridge having non-negative labels only. This can be seen as a degenerate version of the generic case displayed in figure 7, where the face f_1 is shrunk into a single vertex. We have a symmetric picture when $s > 0$ and $t = 0$. Finally, if $s = t = 0$, we apply the Miermont bijection with $p = 1$ source only (equivalent to the Schaeffer bijection), namely v_3, and delay $\tau_3 = -u$. We then obtain a well-labeled tree on which the vertices v_1 and v_2 have label 0 and the branch

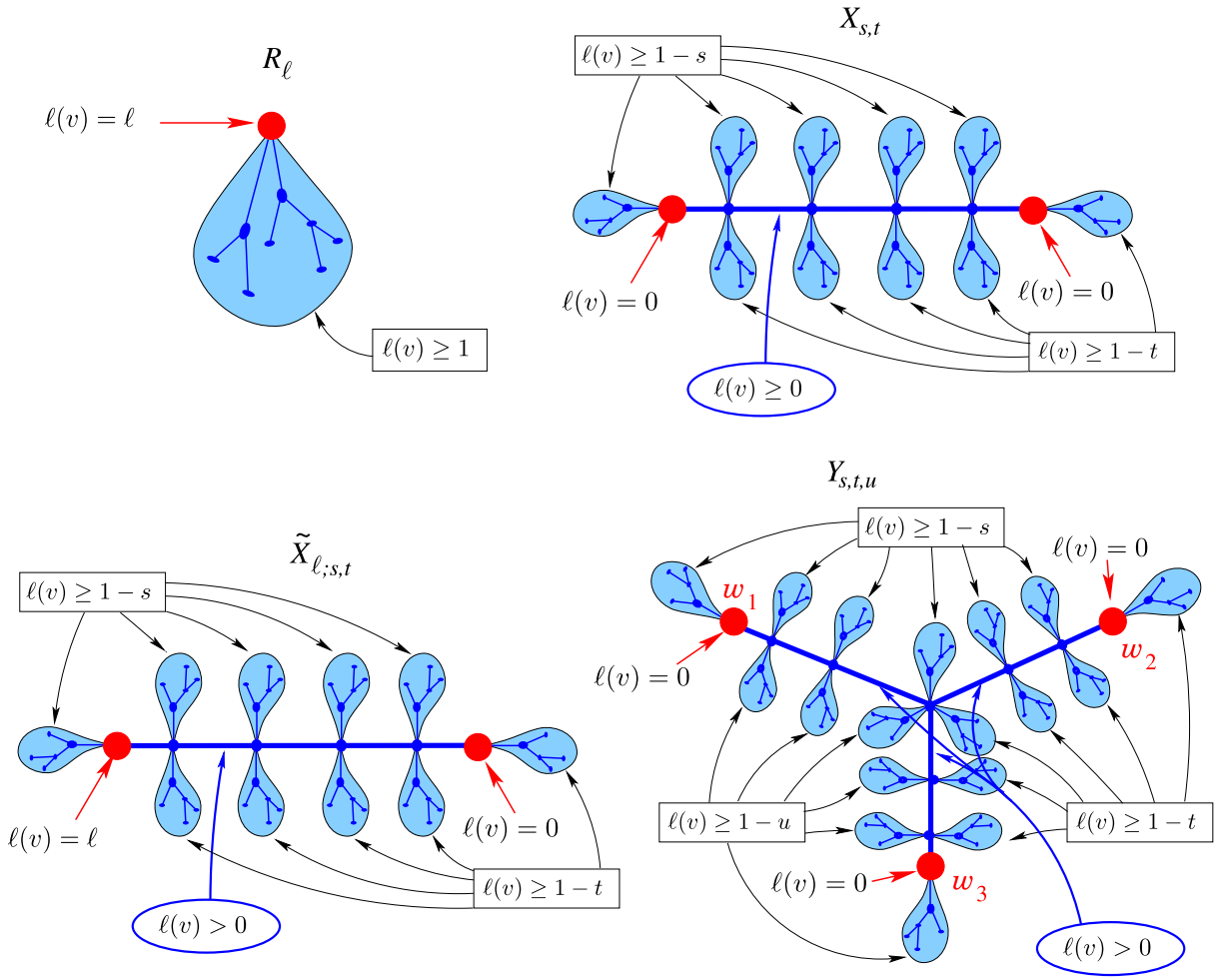

Figure 9. A schematic picture of the known generating functions R_ℓ, $X_{s,t}$, $\tilde{X}_{\ell;s,t}$ and $Y_{s,t,u}$ (see the text).

connecting them has non-negative labels. Again this is a degenerate case of the generic situation in which both f_1 and f_2 degenerate to single vertices.

To conclude, triply pointed quadrangulations with prescribed values of d_{12}, d_{13} and l_{123} are in one-to-one correspondence with well-labeled maps of the generic type displayed in figure 7, or of its degenerate versions displayed in figure 8.

2.2. Generating functions

2.2.1. Known generating functions. We can now readily relate the generating functions of the various well-labeled maps above to those introduced in [15]. As usual, we attach a weight g to each edge of a well-labeled map, which amounts to a weight g per face of the quadrangulation. The first generating function is that of well-labeled trees planted at a corner with label $\ell > 0$ and whose labels are all larger than or equal to 1 (see figure 9). It reads [9]

$$R_\ell = R \frac{[\ell]_x \, [\ell+3]_x}{[\ell+1]_x \, [\ell+2]_x}, \tag{2.10}$$

where

$$[\ell]_x \equiv \frac{1-x^\ell}{1-x}, \tag{2.11}$$

and where

$$\begin{aligned} R &= \frac{1-\sqrt{1-12g}}{6g}, \\ x &= \frac{1-24g-\sqrt{1-12g}+\sqrt{6}\sqrt{72g^2+6g+\sqrt{1-12g}-1}}{2(6g+\sqrt{1-12g}-1)}. \end{aligned} \tag{2.12}$$

Note that $R_\ell = 1+\mathcal{O}(g)$ for all $\ell \geq 1$, with a conventional weight 1 for the tree reduced to a single vertex. The generating function of well-labeled trees planted at a corner with label $\ell \geq 0$ and whose labels are all larger than or equal to $1-s$, for some $s>0$, is then simply given by $R_{\ell+s}$, as obtained by a simple shift of all labels by s.

The second generating function is that of well-labeled trees with two distinct marked vertices having label 0, connected by a branch with non-negative labels only, and such that the trees attached to one side of the branch have labels larger than or equal to $1-s$ and those attached to the other side have labels larger than or equal to $1-t$, with $s>0$ and $t>0$ (see figure 9). By convention, the trees attached to the marked vertices are assumed to be on opposite sides, so that the result is symmetric in s and t. This generating function reads [15]

$$X_{s,t} = \sum_{m\geq 0} \sum_{\substack{\mathcal{M}=(0=\ell_0,\ell_1,\ldots,\ell_m=0) \\ \text{s.t. } \ell_i\geq 0, |\ell_{i+1}-\ell_i|\leq 1, i=0,\ldots,m-1}} \prod_{k=0}^{m-1} g\, R_{\ell_k+s}\, R_{\ell_k+t} = \frac{[3]_x\,[s+1]_x\,[t+1]_x\,[s+t+3]_x}{[1]_x\,[s+3]_x\,[t+3]_x\,[s+t+1]_x}. \tag{2.13}$$

Note that $X_{s,t} = 1+\mathcal{O}(g)$, with a conventional weight 1 for the tree reduced to a single vertex, which is added for convenience to the family of trees enumerated by $X_{s,t}$.

We may instead consider well-labeled trees with two marked vertices, one with label $\ell>0$, the other with label 0, with *strictly positive* labels on the branch in between and such that the trees attached to one side have labels larger than or equal to $1-s$ and those attached to the other side have labels larger than or equal to $1-t$, with $s>0$ and $t>0$ (see figure 9). The tree attached to the extremity with label ℓ is assumed to have labels larger than or equal to $1-s$ and that attached to the extremity with label 0 is assumed to have labels larger than or equal to $1-t$. The resulting generating function reads [15]

$$\begin{aligned} \tilde{X}_{\ell;s,t} &= \sum_{m\geq \ell} \sum_{\substack{\mathcal{M}=(\ell=\ell_0,\ell_1,\ldots,\ell_m=0) \\ \text{s.t. } \ell_i>0, |\ell_{i+1}-\ell_i|\leq 1, i=0,\ldots,m-1}} g\, R_{\ell+s} R_t \prod_{k=1}^{m-1} g\, R_{\ell_k+s}\, R_{\ell_k+t} \\ &= \frac{x^\ell\,[s+1]_x\,[s+2]_x\,[t]_x\,[t+3]_x\,[2\ell+s+t+3]_x}{[s+t+3]_x\,[\ell+s+1]_x\,[\ell+s+2]_x\,[\ell+t]_x\,[\ell+t+3]_x}. \end{aligned} \tag{2.14}$$

This last formula extends to $\ell=0$ where it yields $X_{0;s,t}=1$, corresponding again to a conventional weight 1 for the tree reduced to a single vertex.

The final generating function counts well-labeled trees with three marked vertices, say w_1, w_2, w_3, and with the following constraints (see figure 9). On the tree, the marked

J. Stat. Mech. (2009) P03001

vertices are connected by three branches joining at a central vertex. We impose that the branches leading respectively to w_1, w_2 and w_3 appear clockwise around this central vertex. We also impose that all labels on these branches be strictly positive, except for w_1, w_2 and w_3, which have label 0. We further impose that trees attached to the branch from w_1 to w_2 on the side opposite to w_3 have labels larger than or equal to $1-s$. Similarly, we impose that trees attached to the branch from w_2 to w_3 (respectively from w_3 to w_1) on the side opposite to w_1 (respectively w_2) have labels larger than or equal to $1-t$ (respectively $1-u$). By convention, the labels on the tree attached to w_1 (respectively w_2 and w_3) are assumed to be larger than or equal to $1-s$ (respectively $1-t$ and $1-u$). The corresponding generating function reads [15]

$$\begin{aligned} Y_{s,t,u} &= \sum_{\ell=0}^{\infty} \tilde{X}_{\ell;s,t} \tilde{X}_{\ell;t,u} \tilde{X}_{\ell;u,s} \\ &= \frac{[s+3]_x\,[t+3]_x\,[u+3]_x\,[s+t+u+3]_x}{[3]_x\,[s+t+3]_x\,[t+u+3]_x\,[u+s+3]_x}. \end{aligned} \tag{2.15}$$

Again, we have $Y_{s,t,u} = 1 + \mathcal{O}(g)$, with a conventional weight 1 for the tree reduced to a single vertex, which is added for convenience to the family of trees enumerated by $Y_{s,t,u}$.

2.2.2. Application to minimal separating loops via the Schaeffer bijection. In this approach, we have to enumerate trees of the type displayed in figure 5. It is convenient to first relax the condition on the global minimum, demanding only that it be larger than or equal to $1-u$. We can then decompose the tree by cutting it at the first and last occurrences of the label 0 on the branch from v_1 to v_2, resulting in three trees counted respectively by $\tilde{X}_{s;u,u}$, $X_{u,u}$ and $\tilde{X}_{t;u,u}$ (see figure 10 for an illustration). The corresponding generating function therefore reads

$$\begin{aligned} H_{\mathrm{loop}}(s,t,u) &= \tilde{X}_{s;u,u}\, X_{u,u}\, \tilde{X}_{t;u,u} \\ &= x^{s+t} \frac{[3]_x\,[u]_x^2\,[u+1]_x^4\,[u+2]_x^2\,[2s+2u+3]_x\,[2t+2u+3]_x}{[1]_x\,[2u+1]_x\,[2u+3]_x \prod_{k=0}^{3} [s+u+k]_x\,[t+u+k]_x}. \end{aligned} \tag{2.16}$$

To restore the condition that the global minimal label be exactly $1-u$, we simply have to consider $\Delta_u H_{\mathrm{loop}}(s,t,u)$ where Δ_u is the finite difference operator:

$$\Delta_u f(u) \equiv f(u) - f(u-1). \tag{2.17}$$

To conclude, the generating function for triply pointed quadrangulations with prescribed values of d_{13}, d_{23} and l_{123} is given by

$$\begin{aligned} &G_{\mathrm{loop}}(d_{13}, d_{23}; l_{123}) = \Delta_u H_{\mathrm{loop}}(s,t,u), \\ &\text{with } s = d_{13} - l_{123}/2, \qquad t = d_{23} - l_{123}/2, \qquad u = l_{123}/2. \end{aligned} \tag{2.18}$$

2.2.3. Application to minimal separating loops via the Miermont bijection. In this approach, we simply have to enumerate maps of the type displayed in figures 7 and 8. Again, we relax the conditions on the minimal label within each face, namely we demand only that it be larger than or equal to $1-s$, $1-t$ or $1-u$ respectively. In the generic case of figure 7, we can now decompose the map by cutting it at the first and last occurrences of

J. Stat. Mech. (2009) P03001

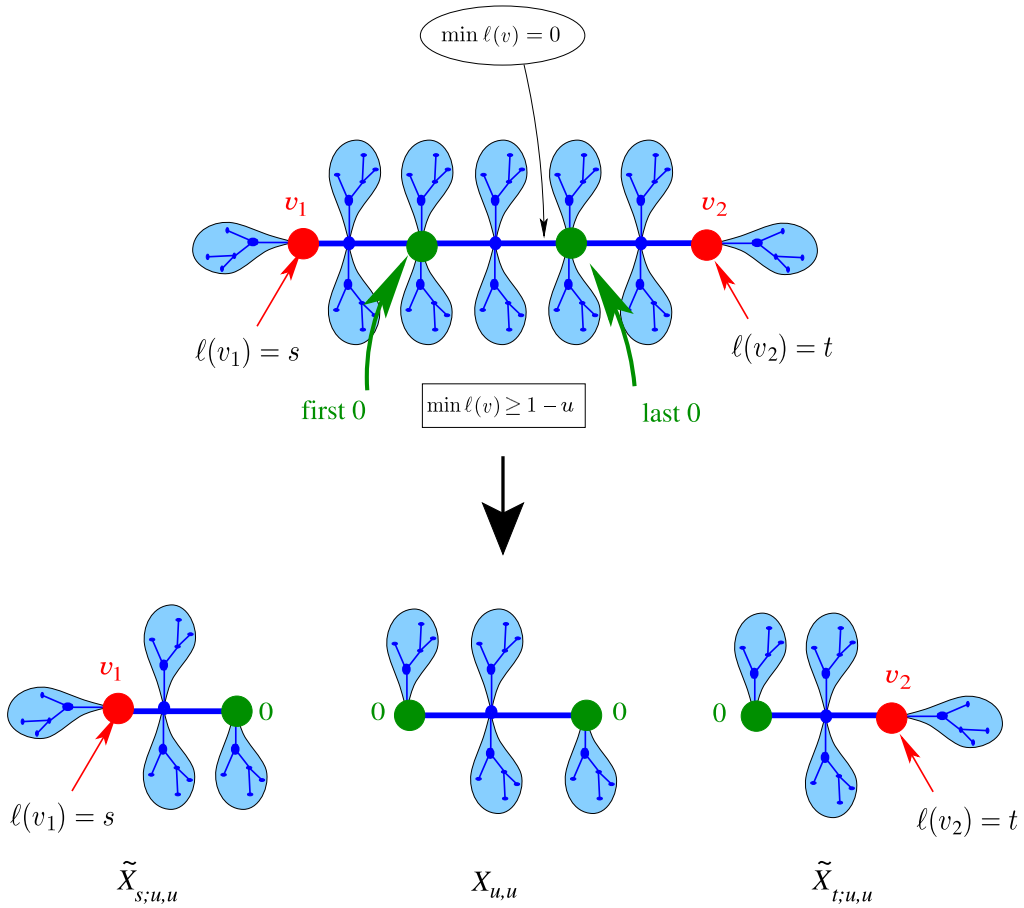

Figure 10. The cutting of a well-labeled tree of the type of figure 5 (with a relaxed constraint on the global minimal label) at the first and last labels 0 encountered along the branch from v_1 to v_2. This results in three pieces, enumerated by $\tilde{X}_{s;u,u}$, $X_{u,u}$ and $\tilde{X}_{t;u,u}$ respectively.

the label 0 on the cycle c_1, starting from the end-point of the bridge b, at the first and last occurrences of the label 0 on the cycle c_2, starting from the other end-point of the bridge b, and finally at the first and last occurrences of the label 0 on the bridge b itself (see figure 11 for an illustration). This results in general in five trees counted respectively by $X_{s,u}$, $Y_{s,u,u}$, $X_{u,u}$, $Y_{t,u,u}$ and $X_{t,u}$. The corresponding generating function therefore reads

$$F_{\rm loop}(s,t,u) = X_{s,u}\, Y_{s,u,u}\, X_{u,u}\, Y_{t,u,u}\, X_{t,u} = \frac{[3]_x\,[s+1]_x\,[t+1]_x\,[u+1]_x^4\,[s+2u+3]_x\,[t+2u+3]_x}{[1]_x^3\,[s+u+1]_x\,[s+u+3]_x\,[t+u+1]_x\,[t+u+3]_x\,[2u+1]_x\,[2u+3]_x}. \tag{2.19}$$

Note that this formula incorporates the cases where some of the cutting points above coincide as we added in $X_{s,t}$ and $Y_{s,t,u}$ the weight 1 of the tree reduced to a single vertex. It also naturally incorporates the degenerate cases of figure 8: for instance, the situation of figure 8(a) is properly taken into account by having the two leftmost trees in the decomposition of figure 11 reduced to single vertices, while the situation of figure 8(b) is

J. Stat. Mech. (2009) P03001

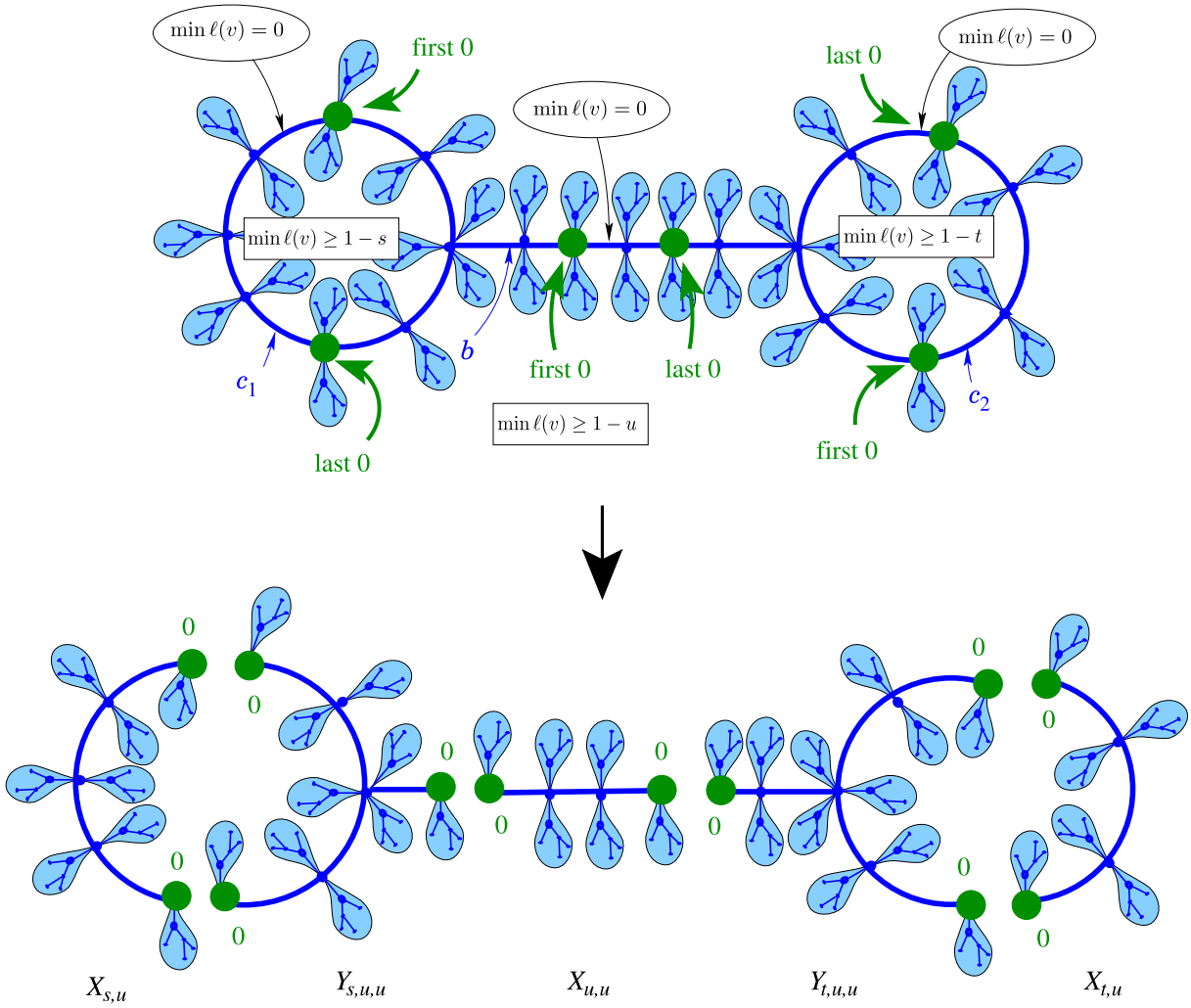

Figure 11. The cutting of a well-labeled map of the type of figure 7 (with relaxed constraints on labels inside each face) at the first and last labels 0 encountered along the cycles c_1, c_2 and the branch b (see the text). This results in five pieces, enumerated by $X_{s,u}$, $Y_{s,u,u}$, $X_{u,u}$, $Y_{t,u,u}$ and $X_{t,u}$ respectively.

properly taken into account by having the two leftmost and the two rightmost trees in the decomposition of figure 11 reduced to single vertices. Again, we can restore the constraint that the minimal label within each face be equal to $1-s$, $1-t$ or $1-u$ respectively by considering $\Delta_s\Delta_t\Delta_u F_{\rm loop}(s,t,u)$. We deduce the alternative formula

$$\begin{aligned} &G_{\rm loop}(d_{13},d_{23};l_{123}) = \Delta_s\Delta_t\Delta_u F_{\rm loop}(s,t,u),\\ &\text{with } s = d_{13}-l_{123}/2, \qquad t = d_{23}-l_{123}/2, \qquad u = l_{123}/2. \end{aligned} \tag{2.20}$$

Note that the two expressions (2.18) and (2.20) are consistent as we have the identity

$$\Delta_s \frac{[s+1]_x\,[s+2u+3]_x}{[s+u+1]_x\,[s+u+3]_x} = x^s \frac{[1]_x\,[u]_x\,[u+2]_x\,[2s+2u+3]_x}{\prod_{k=0}^{3}[s+u+k]_x}, \tag{2.21}$$

which can be checked directly from the definition (2.11).

J. Stat. Mech. (2009) P03001

A simpler generating function is that of triply pointed quadrangulations with a prescribed value of l_{123} only. The corresponding generating function $G_{\rm loop}(l_{123})$ is obtained by summing $G_{\rm loop}(d_{13}, d_{23}; l_{123})$ over all the allowed values of d_{13} and d_{23} for a fixed l_{123}. This amounts to a summation over all non-negative values of s and t, which is easily performed upon using the expression (2.20) by noting that, with the above expression (2.19), the quantities $F_{\rm loop}(-1, t, u)$ and $F_{\rm loop}(s, -1, u)$ vanish identically, so we have

$$\begin{aligned} G_{\rm loop}(l_{123}) &= \Delta_u F_{\rm loop}(\infty, \infty, u) \\ &= \Delta_u \frac{[3]_x\,[u+1]_x^4}{[1]_x^3\,[2u+1]_x\,[2u+3]_x}, \qquad \text{with } u = l_{123}/2. \end{aligned} \tag{2.22}$$

2.3. Continuum limit

The scaling limit is obtained by letting g approach its critical value $1/12$ and considering large values of d_{13}, d_{23} and l_{123} with the following scaling:

$$g = \tfrac{1}{12}\,(1 - \Lambda\,\epsilon) \qquad d_{13} = D_{13}\epsilon^{-1/4}, \qquad d_{23} = D_{23}\epsilon^{-1/4}, \qquad l_{123} = L_{123}\epsilon^{-1/4}, \tag{2.23}$$

and $\epsilon \to 0$. The quantity Λ may be interpreted as a 'cosmological constant'. In this limit, we have

$$\begin{aligned} &G_{\rm loop}(l_{123}) \sim \epsilon^{-1/4} 2\,\mathcal{G}_{\rm loop}(L_{123}; \alpha), \qquad \text{where} \\ &\mathcal{G}_{\rm loop}(L_{123}; \alpha) = \frac{1}{2}\partial_U\,\frac{3}{\alpha^2}\frac{\sinh^4(\alpha U)}{\sinh^2(2\alpha U)}\bigg|_{U=L_{123}/2} = \frac{3}{4\alpha}\frac{\sinh(\alpha L_{123}/2)}{\cosh^3(\alpha L_{123}/2)}. \end{aligned} \tag{2.24}$$

Here and throughout the paper, we use the notation

$$\alpha = \sqrt{3/2}\Lambda^{1/4}. \tag{2.25}$$

Note the factor $1/2$ in the definition of $\mathcal{G}_{\rm loop}$, which is introduced to compensate for the fact that, at the discrete level, l_{123} can take only even integer values. More generally, we have

$$\begin{aligned} &G_{\rm loop}(d_{12}, d_{13}, l_{123}) \sim \epsilon^{1/4} 2\,\mathcal{G}_{\rm loop}(D_{12}, D_{13}, L_{123}; \alpha), \\ &F_{\rm loop}(s, t, u) \sim \epsilon^{-1/2}\mathcal{F}_{\rm loop}(S, T, U; \alpha), \\ &H_{\rm loop}(s, t, u) \sim \mathcal{H}_{\rm loop}(S, T, U; \alpha), \end{aligned} \tag{2.26}$$

where

$$\begin{aligned} \mathcal{F}_{\rm loop}(S, T, U; \alpha) &= \frac{3}{\alpha^2}\frac{\sinh(\alpha S)\sinh(\alpha T)\sinh^4(\alpha U)\sinh(\alpha(S+2U))\sinh(\alpha(T+2U))}{\left(\sinh(\alpha(S+U))\sinh(\alpha(T+U))\sinh(2\alpha U)\right)^2}, \\ \mathcal{H}_{\rm loop}(S, T, U; \alpha) &= 3\frac{\sinh^8(\alpha U)\sinh(2\alpha(S+U))\sinh(2\alpha(T+U))}{\sinh^2(2\alpha U)\sinh^4(\alpha(S+U))\sinh^4(\alpha(T+U))}, \end{aligned} \tag{2.27}$$

and where

$$\begin{aligned} &\mathcal{G}_{\rm loop}(D_{12}, D_{23}, L_{123}; \alpha) = \tfrac{1}{2}\partial_S\partial_T\partial_U\mathcal{F}_{\rm loop}(S, T, U; \alpha) = \tfrac{1}{2}\partial_U\mathcal{H}_{\rm loop}(S, T, U; \alpha), \\ &\text{with } S = D_{13} - L_{123}/2, \qquad T = D_{23} - L_{123}/2, \qquad U = L_{123}/2. \end{aligned} \tag{2.28}$$

J. Stat. Mech. (2009) P03001

Again the two expressions above for $\mathcal{G}_{\rm loop}(D_{12}, D_{23}, L_{123}; \alpha)$ are consistent as we have the identity

$$\partial_S \left(\frac{1}{\alpha} \frac{\sinh(\alpha S)\sinh(\alpha(S+2U))}{\sinh^2(\alpha(S+U))} \right) = \frac{\sinh^2(\alpha U)\sinh(2\alpha(S+U))}{\sinh^4(\alpha(S+U))}, \qquad (2.29)$$

which is the continuous counterpart of (2.21).

The above continuous formulae can be used to capture the statistical properties of triply pointed quadrangulations with *fixed size*, i.e. with a fixed number n of faces, in the limit $n \to \infty$. Indeed, fixing n amounts to extracting the g^n term of the various discrete generating functions at hand. This can be done via a contour integral in g which, at large n, translates via a saddle point estimate into an integral over a real variable ξ. More precisely, considering for instance the generating function $G_{\rm loop}(l_{123})$, we write

$$G_{\rm loop}(l_{123})|_{g^n} = \frac{1}{2{\rm i}\pi} \oint \frac{{\rm d}g}{g^{n+1}} G_{\rm loop}(l_{123}), \qquad (2.30)$$

and we perform the change of variables

$$g = \frac{1}{12}\left(1 + \frac{\xi^2}{n}\right), \qquad l_{123} = L_{123}\, n^{1/4}. \qquad (2.31)$$

At large n, the contour integral becomes at dominant order an integral over real values of ξ and we can use the continuous formulae above with $\epsilon = 1/n$ and $\lambda = -\xi^2$. After a proper normalization by the number of triply pointed quadrangulations with fixed size n, we obtain the probability density $\rho_{\rm loop}(L_{123})$ for the rescaled length L_{123}:

$$\rho_{\rm loop}(L_{123}) = \frac{2}{{\rm i}\sqrt{\pi}} \int_{-\infty}^{\infty} {\rm d}\xi\, \xi\, {\rm e}^{-\xi^2}\, \mathcal{G}_{\rm loop}(L_{123}; \sqrt{-3{\rm i}\xi/2}). \qquad (2.32)$$

The quantity $\rho_{\rm loop}(L_{123})\, {\rm d}L_{123}$ is the infinitesimal probability that the (rescaled) minimal length for loops having origin v_3 and separating v_1 from v_2 lies in the range $[L_{123}, L_{123} + {\rm d}L_{123}]$ in the ensemble of triply pointed quadrangulations with fixed size n, in the limit $n \to \infty$. This probability density is plotted in figure 12 and has the following limiting behaviors:

$$\begin{aligned} &\rho_{\rm loop}(L_{123}) \sim \tfrac{3}{16} L_{123}^3 \qquad \text{when } L_{123} \to 0, \\ &\rho_{\rm loop}(L_{123}) \sim \frac{1}{6^{1/6}} L_{123}^{2/3} {\rm e}^{-\left(\frac{3}{4}\right)^{5/3} L_{123}^{4/3}} \qquad \text{when } L_{123} \to \infty. \end{aligned} \qquad (2.33)$$

The associated average value of L_{123} reads

$$\langle L_{123} \rangle = \tfrac{4}{3} \langle D \rangle = 2.361\,98\ldots \qquad \text{with } \langle D \rangle = 2\sqrt{\frac{3}{\pi}}\Gamma\left(\frac{5}{4}\right) = 1.771\,48\ldots. \qquad (2.34)$$

Here and throughout the paper, we decide to express average distances in units of the average distance $\langle D \rangle$ between two uniformly chosen vertices in a large quadrangulation, whose value given above was computed in [19]–[21].

Similarly, the joint probability density for $D_{13} = d_{13}/n^{1/4}$, $D_{23} = d_{23}/n^{1/4}$ and L_{123} reads

$$\rho_{\rm loop}(D_{12}, D_{13}, L_{123}) = \frac{2}{{\rm i}\sqrt{\pi}} \int_{-\infty}^{\infty} {\rm d}\xi\, \xi\, {\rm e}^{-\xi^2}\, \mathcal{G}_{\rm loop}(D_{12}, D_{13}, L_{123}; \sqrt{-3{\rm i}\xi/2}), \qquad (2.35)$$

J. Stat. Mech. (2009) P03001

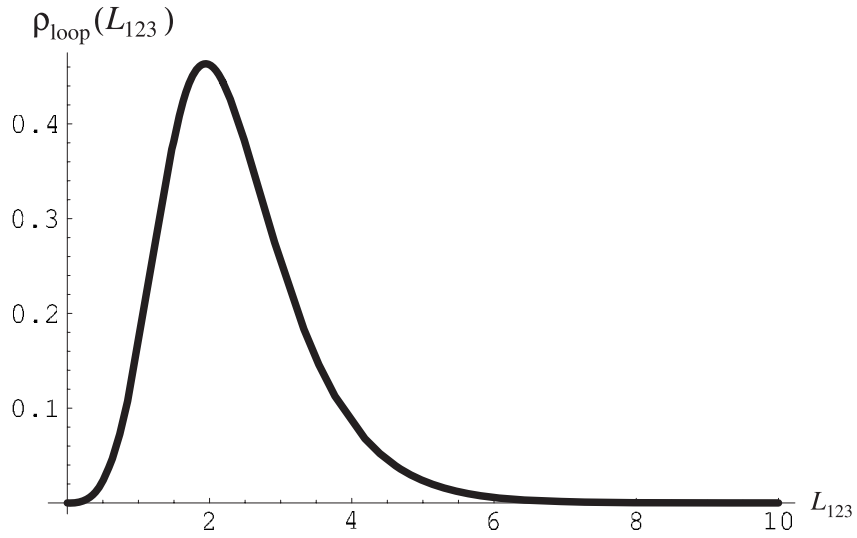

Figure 12. Plot of the probability density $\rho_{\rm loop}(L_{123})$.

while the conditional probability density for D_{13} and D_{23}, given the value of L_{123}, simply reads

$$\rho_{\rm loop}(D_{12}, D_{13}|L_{123}) = \frac{\rho_{\rm loop}(D_{13}, D_{23}, L_{123})}{\rho_{\rm loop}(L_{123})}. \tag{2.36}$$

This conditional probability density is represented in figure 13 for decreasing values of L_{123} (namely $L_{123} = 2.0$, 1.6 and 1.0), and in figure 14 for increasing values of L_{123} (namely $L_{123} = 2.0$, 3.0 and 4.0). For large enough L_{123}, this joint probability density is maximal for equal values of D_{13} and D_{23}, i.e. when the two vertices v_1 and v_2 are equally distant from v_3. In contrast, for small enough L_{123}, we observe a symmetry breaking phenomenon with a probability density being maximal when one of the two vertices v_1 or v_2 lies closer from v_3 than the other.

This phenomenon increases for smaller L_{123} and, when $L_{123} \to 0$, we find that

$$\rho_{\rm loop}(D_{13}, D_{23}|L_{123}) \sim \rho(D_{13}) \times \frac{2}{L_{123}} \psi\left(\frac{2D_{23}}{L_{123}}\right) + \rho(D_{23}) \times \frac{2}{L_{123}} \psi\left(\frac{2D_{13}}{L_{123}}\right), \tag{2.37}$$

with a scaling function

$$\psi(\omega) = \frac{3}{4} \frac{2\omega - 1}{\omega^4} \tag{2.38}$$

normalized to 1/2 when ω varies from 1 to ∞, and where $\rho(D)$ is the so-called *canonical two-point function*, which is the probability density for the distance D between two vertices picked uniformly at random in a large quadrangulation. This canonical two-point function is given by a formula similar to (2.32):

$$\begin{aligned} &\rho(D) = \frac{2}{{\rm i}\sqrt{\pi}} \int_{-\infty}^{\infty} {\rm d}\xi\, \xi\, {\rm e}^{-\xi^2}\, \mathcal{G}(D; \sqrt{-3{\rm i}\xi/2}), \\ &\text{with } \mathcal{G}(D;\alpha) = 4\alpha^3 \frac{\cosh(\alpha D)}{\sinh^3(\alpha D)}. \end{aligned} \tag{2.39}$$

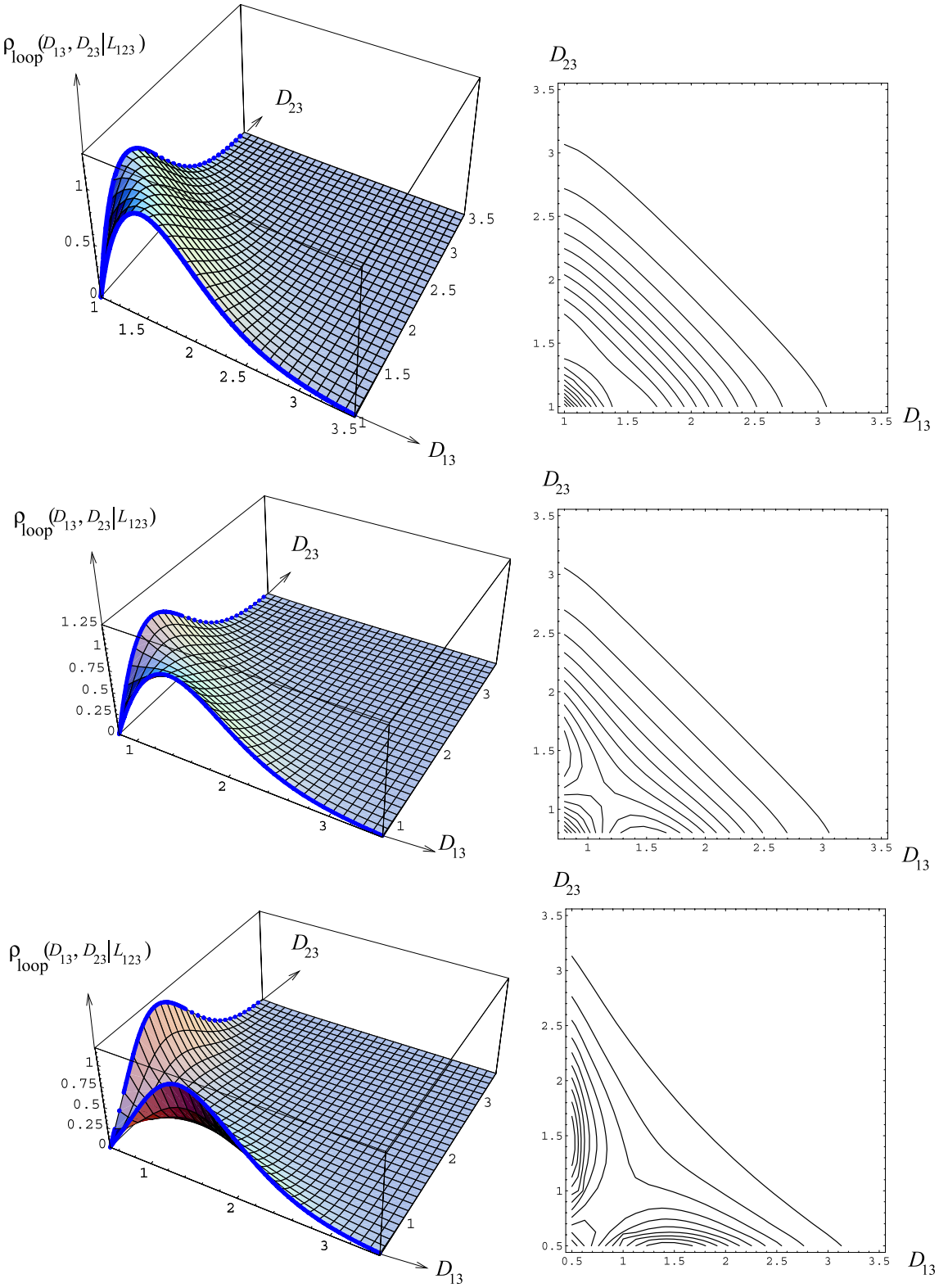

Figure 13. Plots of the conditional probability density $\rho_{\text{loop}}(D_{13}, D_{23}|L_{123})$ for $L_{123} = 2.0$, 1.6 and 1.0, from top to bottom. For each plot on the left, we display its associated contour plot on the right.

doi:10.1088/1742-5468/2009/03/P03001

J. Stat. Mech. (2009) P03001

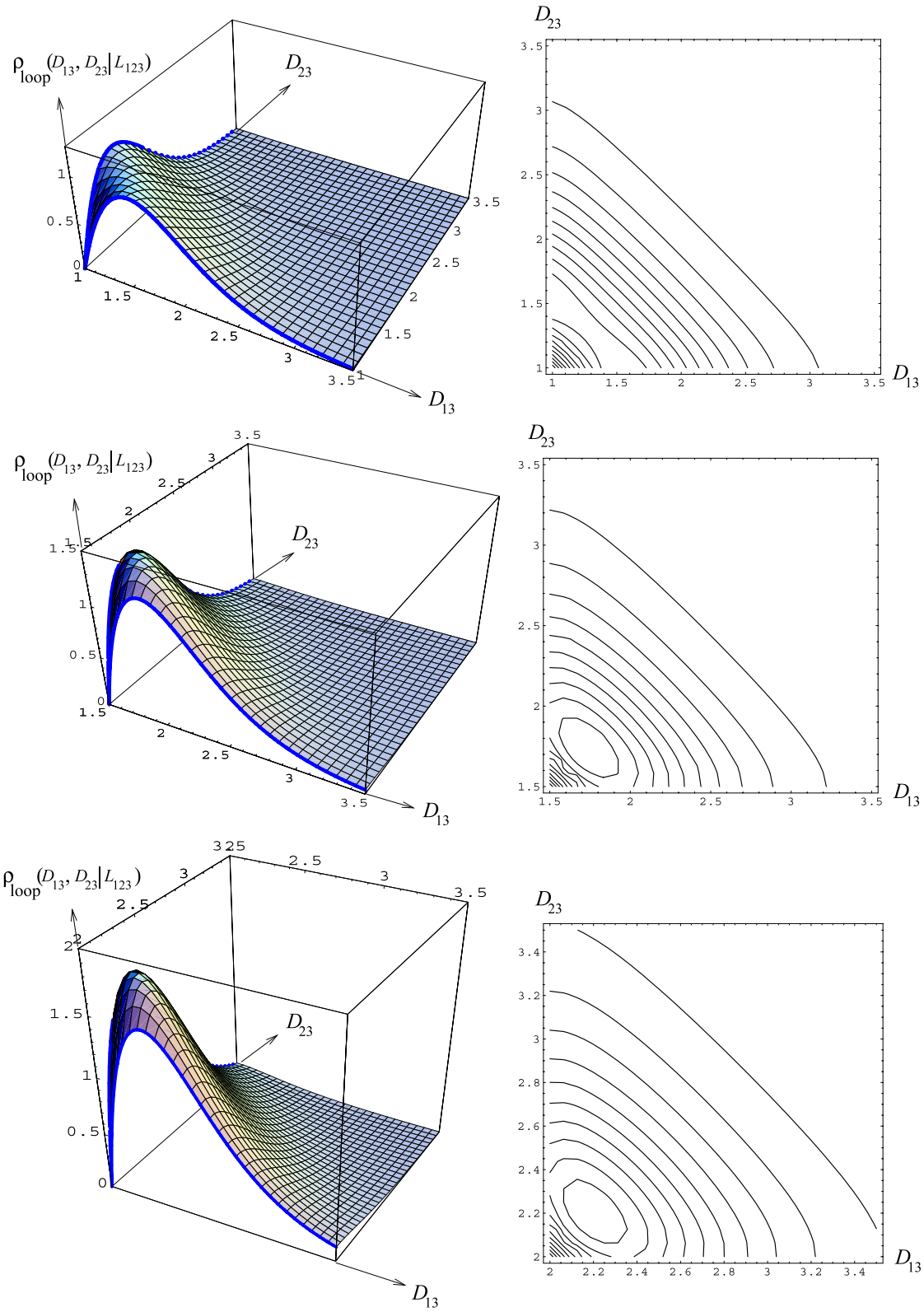

Figure 14. Plots of the conditional probability density $\rho_{\mathrm{loop}}(D_{13}, D_{23}|L_{123})$ for $L_{123} = 2.0$, 3.0 and 4.0, from top to bottom.

doi:10.1088/1742-5468/2009/03/P03001

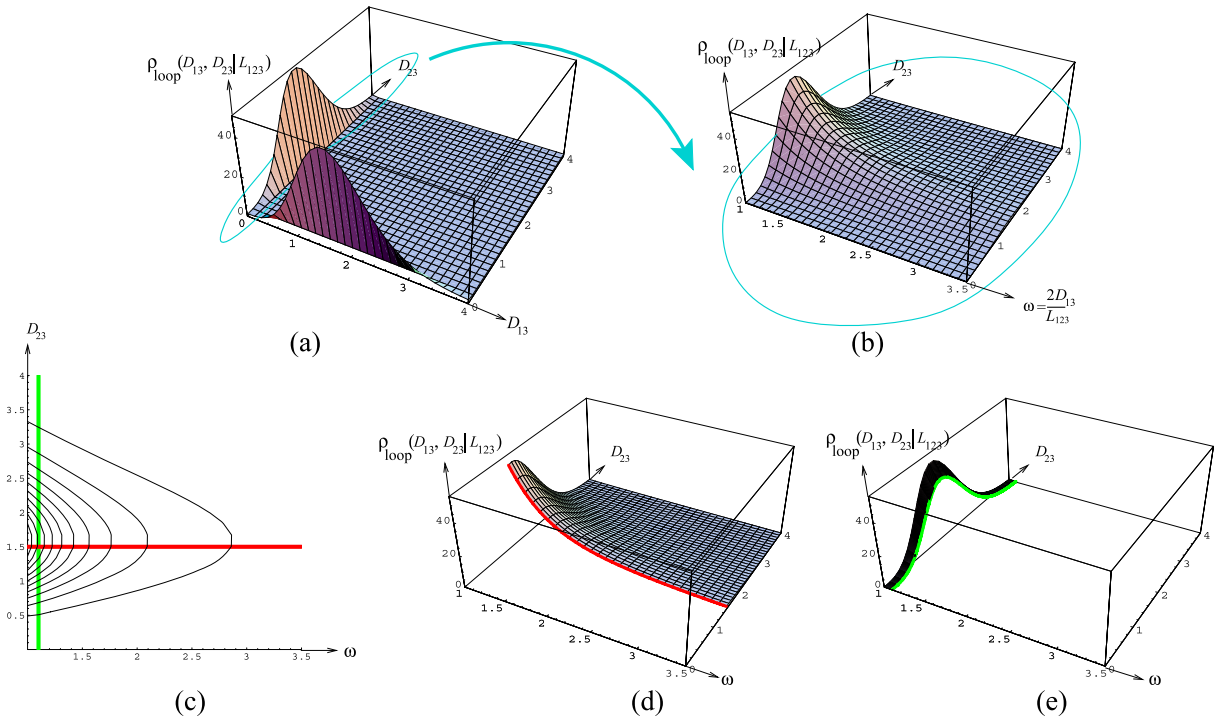

Figure 15. (a) Plot of the conditional probability density $\rho_{\mathrm{loop}}(D_{13}, D_{23}|L_{123})$ for a small value of L_{123}, here $L_{123} = 0.02$. This density is concentrated in two regions corresponding to either D_{13} or D_{23} being of order L_{123}. A zoom on the first region is obtained by considering the same plot (b) with a rescaled abscissa $\omega = 2D_{13}/L_{123}$, or the corresponding contour plot (c). As is apparent by taking longitudinal and transverse cut views along the thick lines in (c), the probability density factorizes in this region into the product of the density $\psi(\omega)$ (red curve in (d)) and the two-point function $\rho(D_{23})$ (green curve in (e)).

The particular form (2.37) expresses that, when L_{123} becomes small, one of two vertices v_1 or v_2, say v_1, necessarily lies in the vicinity of v_3, with a distance D_{13} of the order of L_{123} and governed by the density (2.38) for $\omega = 2D_{13}/L_{123}$, while the other vertex lies at an arbitrary distance from the two others, with a probability density given simply by the two-point function of quadrangulations, as expected. This behavior is depicted in figure 15, for $L_{123} = 0.02$. This result corroborates the known property of quadrangulations of large size n: small loops of length negligible with respect to $n^{1/4}$ in the quadrangulation necessarily separate it into a macroscopic domain containing most of the area of the quadrangulation, and a small part of negligible size with respect to n.

In the other limit, i.e. when L_{123} becomes large, we find the limiting behavior

$$\rho_{\mathrm{loop}}(D_{13}, D_{23}|L_{123}) \sim \left(\frac{9L_{123}}{2}\right)^{2/3} \Phi(\mu, \nu),$$
$$\text{with } \mu = \left(D_{13} - \frac{L_{123}}{2}\right)\left(\frac{9L_{123}}{2}\right)^{1/3}, \qquad \nu = \left(D_{23} - \frac{L_{123}}{2}\right)\left(\frac{9L_{123}}{2}\right)^{1/3}, \tag{2.40}$$

J. Stat. Mech. (2009) P03001

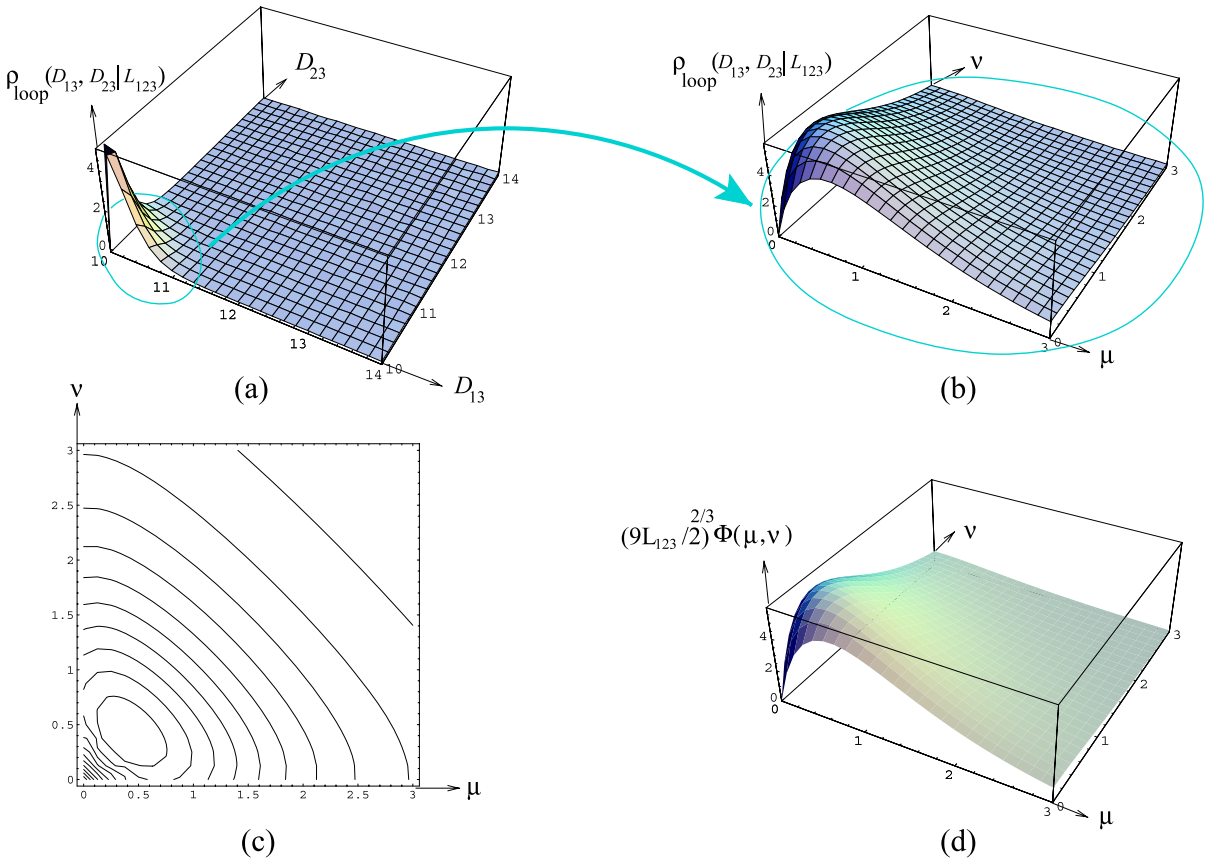

Figure 16. (a) Plot of the conditional probability density $\rho_{\mathrm{loop}}(D_{13}, D_{23}|L_{123})$ for a large value of L_{123}, here $L_{123} = 20.0$. The same plot (b) and its contour (c) in the rescaled variables $\mu = (D_{13} - L_{123}/2)(9L_{123}/2)^{1/3}$ and $\nu = (D_{23} - L_{123}/2)(9L_{123}/2)^{1/3}$. In these variables, the conditional probability density tends to a limiting distribution $\Phi(\mu, \nu)$, as shown in (d).

with a scaling function

$$\Phi(\mu, \nu) = \mathrm{e}^{-(\mu+\nu)} \left(2 - \mathrm{e}^{-\mu} - \mathrm{e}^{-\nu}\right) \tag{2.41}$$

properly normalized to 1 when μ and ν vary from 0 to ∞. At large L_{123}, both distances D_{13} and D_{23} are therefore necessarily of order $L_{123}/2$, with differences $D_{13} - L_{123}/2$ and $D_{23} - L_{123}/2$ of order $L_{123}^{-1/3}$, governed by the joint probability density (2.41). This behavior is depicted in figure 16 for $L_{123} = 20.0$.

3. Confluence

3.1. Confluence of geodesics

In this section, we explain how we can use the quantities computed in section 2, or slight generalizations of them, to study the phenomenon of *confluence of geodesics* in the scaling limit of large quadrangulations. It was shown by Le Gall [14] and Miermont [13] that two typical points in a large random quadrangulation are joined by a unique 'macroscopic'

J. Stat. Mech. (2009) P03001

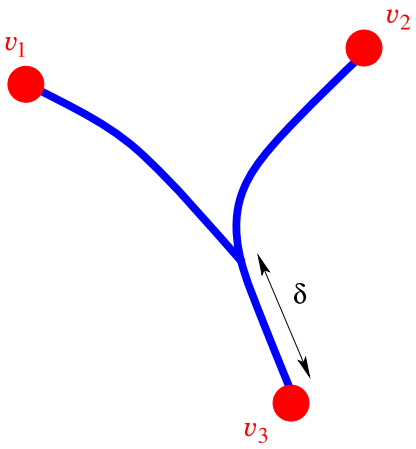

Figure 17. A schematic picture of the phenomenon of confluence of geodesics. For generic points v_1, v_2 and v_3 and in the scaling limit of large quadrangulations, the geodesic from v_1 to v_3 and that from v_2 to v_3 (represented as thick blue lines) are unique and have a common part of macroscopic length δ.

geodesic path. By this, it is meant that, although there are a large (extensive in the length) number of geodesic paths between two points at a discrete level, all these geodesics remain within a distance negligible with respect to $n^{1/4}$, which is the scale at which points can be distinguished in the scaling limit. Moreover, given three typical vertices v_1, v_2 and v_3, the unique macroscopic geodesic from v_1 to v_3 and the unique macroscopic geodesic from v_2 to v_3 merge before reaching v_3, i.e. have a macroscopic common part (see figure 17). This is the phenomenon of confluence of geodesics [14] which raises interesting problems, such as that of the distribution of the length δ of this common part.

3.1.1. Approach via the Schaeffer bijection. At a discrete level, this length can be estimated by a particular choice of geodesics defined as follows: we start again with a triply pointed quadrangulation with marked vertices v_1, v_2 and v_3 and consider the associated well-labeled tree obtained from the Schaeffer bijection, taking v_3 has the origin. This tree has two marked vertices v_1 and v_2, and upon shifting the labels so that the minimal label on the branch between v_1 and v_2 is 0, it is of the type displayed in figure 5 for some s, t and u. We can now consider the *leftmost* geodesic from v_1 to v_3 formed by the chain of successors from the corner incident to v_1 and lying immediately on the right of the branch oriented from v_1 to v_2. Similarly, we consider the leftmost geodesic from v_2 to v_3 obtained as the chain of successors from the corner incident to v_2 and lying immediately on the left of the branch (oriented again from v_1 to v_2). These two geodesics will merge at a point which we characterize as follows (see figure 18 for an illustration): let us call $1-u'$ (respectively $1-u''$) the minimal label on trees attached to the left (respectively right) side of the branch oriented from v_1 to v_2 (with the convention that the tree attached to v_1 lies on the left side of the branch, and that attached to v_2 on the right side), with $u = \max(u', u'')$. Then the two chosen geodesics have a common part of length $|u' - u''|$. Indeed, assuming without loss of generality that $u = u' \geq u''$, all the $s + u$ successors of the corner chosen at v_1 lie on the left of the branch until v_3 (with label $-u$) is reached. On the other hand, among

J. Stat. Mech. (2009) P03001

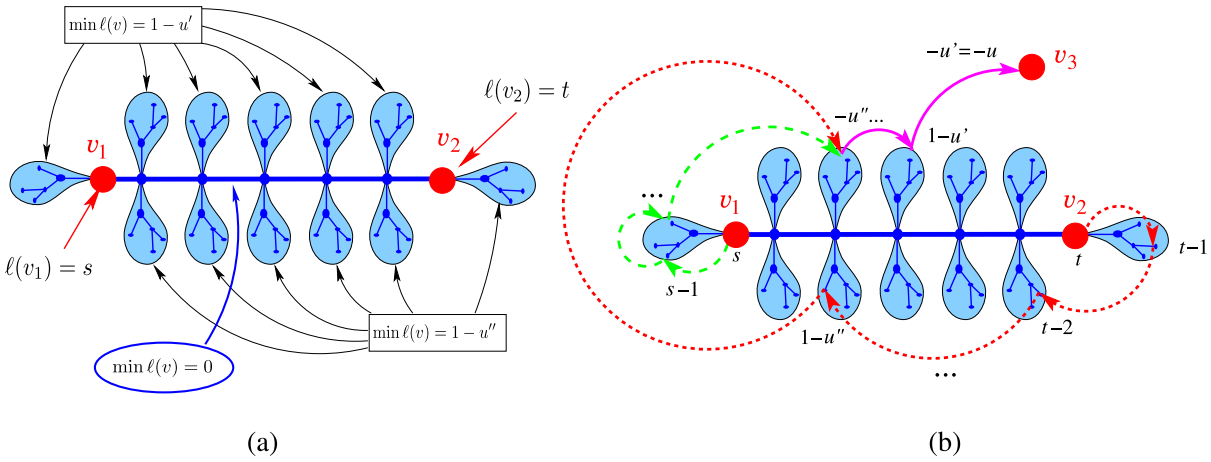

Figure 18. In the well-labeled tree of figure 5, we distinguish (a) the minimal label $1-u'$ on trees attached to one side of the branch from v_1 to v_2 and the minimal label $1-u''$ on trees attached to the other side of the branch, with $u=\max(u',u'')$. The quantity $|u'-u''|$ measures the length of the common part of the leftmost geodesics from v_1 and v_2 to the added vertex v_3. As apparent in (b), here in the case $u'>u''$, these leftmost geodesics are made of two distinct chains of successors of respective lengths $s-u''$ (green long-dashed arrows) and $t-u''$ (red short-dashed arrows), followed by a common chain of successors of length $u'-u''$ (magenta solid arrows).

the $t+u$ successors of the corner chosen at v_2, the first $t+u''-1$ successors are found on the right of the branch but the $(t+u'')$th successor, having label $-u''$, is on the left of the branch and coincides with the $(s+u'')$th successor of the corner chosen at v_1. From that point, all remaining successors form a common part of length $u'-u''$ (see figure 18). To conclude, there is a correspondence between, on the one hand, well-labeled trees with fixed values of s, t, u' and u'' as defined above and, on the other hand, triply pointed quadrangulations with prescribed values $d_{13}=s+\max(u',u'')$, $d_{23}=t+\max(u',u'')$, $l_{123}=2\max(u',u'')$ and such that the leftmost geodesics from v_1 to v_3 and from v_2 to v_3 have a common part of length $|u'-u''|$. Note that the sign of $u'-u''$ simply accounts for the relative position of the geodesics: when $u'>u''$ (respectively $u''>u'$), the geodesic from v_1 to v_3 merges on the right (respectively on the left) of the geodesic from v_2 to v_3.

We now wish to enumerate the above trees. By an immediate generalization of equation (2.16), such trees have the generating function

$$\Delta_{u'}\Delta_{u''}H_{\mathrm{loop}}(s,t,u',u'') \qquad \text{where } H_{\mathrm{loop}}(s,t,u',u'')=\tilde{X}_{s;u',u''}\,X_{u',u''}\,\tilde{X}_{t;u'',u'}. \tag{3.1}$$

In the scaling limit, this generating function becomes

$$\partial_{U'}\partial_{U''}\mathcal{H}_{\mathrm{loop}}(S,T,U',U'';\alpha), \qquad \text{where}$$
$$\mathcal{H}_{\mathrm{loop}}(S,T,U',U'';\alpha)=$$
$$3\frac{\sinh^4(\alpha U')\sinh^4(\alpha U'')\sinh(\alpha(2S+U'+U''))\sinh(\alpha(2T+U'+U''))}{(\sinh(\alpha(U'+U''))\sinh(\alpha(S+U'))\sinh(\alpha(S+U''))\sinh(\alpha(T+U'))\sinh(\alpha(T+U')))^2}, \tag{3.2}$$

J. Stat. Mech. (2009) P03001

and we expect that any other choice for the geodesics at the discrete level would lead to the same continuous expression. This formula holds in the grand canonical formalism and can be transformed via an integral of the type (2.32) into the canonical normalized joint probability density for D_{13}, D_{23}, L_{123} and the (rescaled) length $\delta \equiv |U' - U''|$ for the common part of the geodesics.

3.1.2. Approach via the Miermont bijection. As in section 2, a useful alternative expression for the above function may be obtained by use of the Miermont bijection for triply pointed quadrangulations, leading, for the special choice (2.8) of delays, to well-labeled maps of the type displayed in figure 7 (or of its degenerate versions) for some s, t, and u. A particular geodesic path from v_1 to v_3 is obtained by picking, say, the last label 0 on the (counterclockwise oriented) cycle c_1, looking at the two corners at that vertex lying immediately on the right of the cycle when we follow the cycle in both directions, and considering the chains of successors of these two corners. The concatenation of these chains forms the desired geodesic path. A similar geodesic path can be considered from v_2 to v_3, passing via the last label 0 on the (counterclockwise oriented) cycle c_2. Let us now call $1 - u'$ the minimal label on trees attached to the left side of the branch b (oriented from v_1 to v_2), to the external side of the cycle c_1 before the last occurrence of a label 0 on this cycle, and to the external side of the cycle c_2 after the last occurrence of a label 0 on this cycle (see figure 19 for an illustration). We also call $1 - u''$ the minimal label on trees attached to the complementary part of the frontier of the face f_3, with $u = \max(u', u'')$. Then by arguments similar to the discussion above, the two particular geodesics have a common part of length $|u' - u''|$. We now have a correspondence between, on the one hand, well-labeled maps with fixed values of s, t, u' and u'' as defined above and, on the other hand, triply pointed quadrangulations with prescribed values $d_{13} = s + \max(u', u'')$, $d_{23} = t + \max(u', u'')$, $l_{123} = 2\max(u', u'')$ and such that the two particular geodesics considered above from v_1 to v_3 and from v_2 to v_3 have a common part of length $|u' - u''|$. By an immediate generalization of equation (2.19), such maps are enumerated by

$$\begin{aligned} &\Delta_s \Delta_t \Delta_{u'} \Delta_{u''} F_{\mathrm{loop}}(s, t, u', u''), \qquad \text{where} \\ &F_{\mathrm{loop}}(s, t, u', u'') = X_{s,u'}\, Y_{s,u'',u'}\, X_{u',u''}\, Y_{t,u',u''}\, X_{t,u''}. \end{aligned} \tag{3.3}$$

Note that this generating function is different from that given by (3.1) as our particular choice of geodesics differs in the Schaeffer and Miermont bijection approaches. In the scaling limit however, we expect to recover the same expression (3.2) due to the unicity of geodesics at a macroscopic level. Indeed, the expression (3.3) translates into

$$\begin{aligned} &\partial_S \partial_T \partial_{U'} \partial_{U''} \mathcal{F}_{\mathrm{loop}}(S, T, U', U''; \alpha), \qquad \text{where} \\ &\mathcal{F}_{\mathrm{loop}}(S, T, U', U''; \alpha) = \\ &\frac{3}{\alpha^2} \frac{\sinh(\alpha S) \sinh(\alpha T) \sinh^2(\alpha U') \sinh^2(\alpha U'') \sinh(\alpha(S + U' + U'')) \sinh(\alpha(T + U' + U''))}{\sinh(\alpha(S + U')) \sinh(\alpha(S + U'')) \sinh(\alpha(T + U')) \sinh(\alpha(T + U'')) \sinh^2(\alpha(U' + U''))}, \end{aligned} \tag{3.4}$$

which precisely matches the continuous expression (3.2), namely

$$\partial_S \partial_T \partial_{U'} \partial_{U''} \mathcal{F}_{\mathrm{loop}}(S, T, U', U''; \alpha) = \partial_{U'} \partial_{U''} \mathcal{H}_{\mathrm{loop}}(S, T, U', U''; \alpha), \tag{3.5}$$

J. Stat. Mech. (2009) P03001

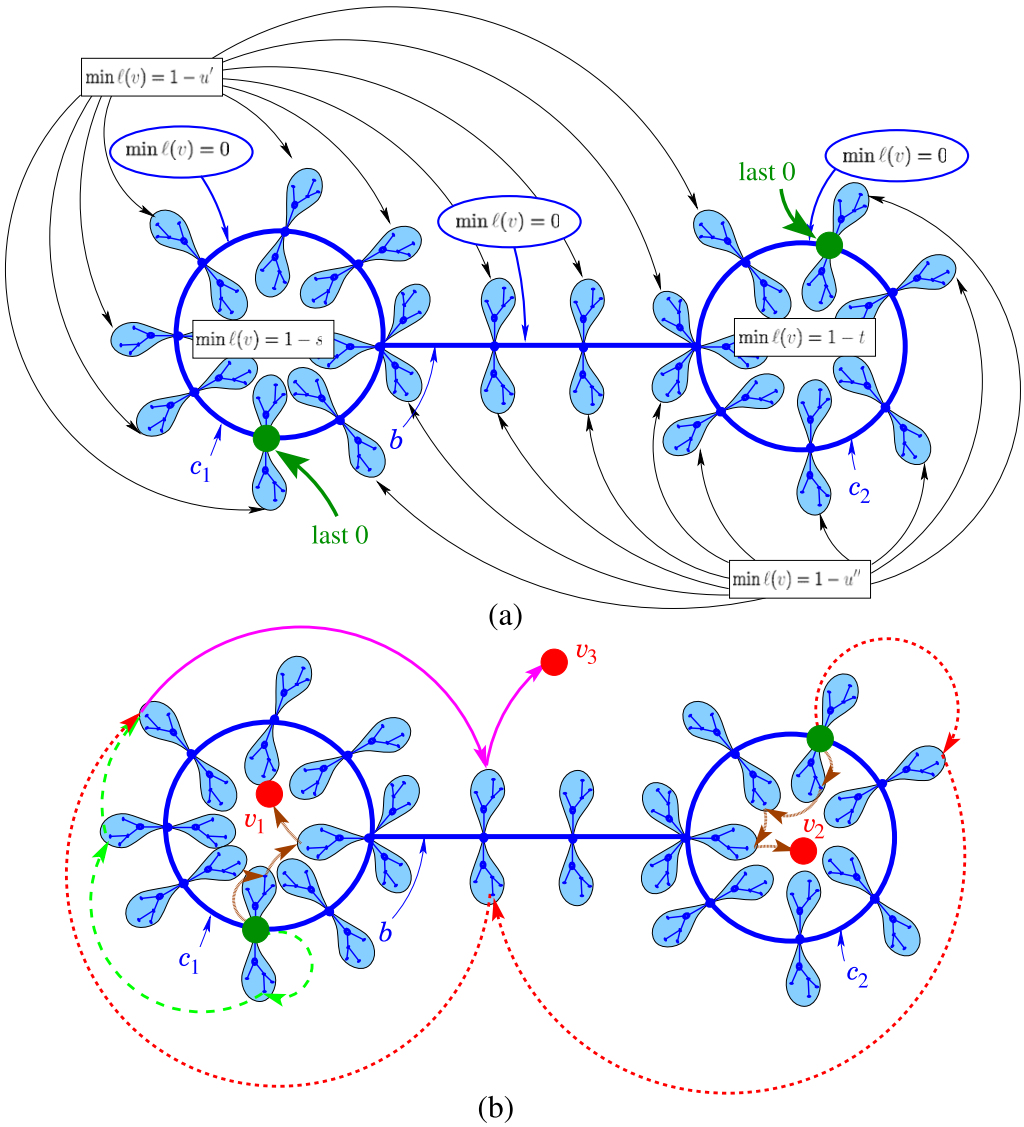

Figure 19. In the well-labeled map of figure 7, we mark the last occurrence of a label 0 on each (counterclockwise oriented) cycle c_1 and c_2 and call $1-u'$ the minimal label on trees attached to the part of the frontier of the external face made of: (i) the left side of the branch b (oriented from c_1 to c_2), (ii) the external side of the cycle c_1 before reaching the marked label 0, and (iii) the external side of the cycle c_2 after passing the marked label 0. We also call $1-u''$ the minimal label on trees attached to the complementary part of the frontier, with $u = \max(u', u'')$. The quantity $|u'-u''|$ measures the length of the common part of two particular geodesics leading from v_1 and v_2 to v_3, as apparent in (b), here in the case $u' > u''$.

as a consequence of the identity

$$\partial_S \left(\frac{1}{\alpha} \frac{\sinh(\alpha S)\sinh(\alpha(S+U'+U''))}{\sinh(\alpha(S+U'))\sinh(\alpha(S+U''))} \right) = \frac{\sinh(\alpha U')\sinh(\alpha U'')\sinh(\alpha(2S+U'+U''))}{\sinh^2(\alpha(S+U'))\sinh^2(\alpha(S+U''))}. \tag{3.6}$$

3.1.3. Marginal law for δ. It is now a simple exercise to obtain, in this scaling limit, the marginal law for δ. We simply have to integrate over all positive values of S, T, U' and U'' with the constraint that $|U'-U''|=\delta$. This is done more easily in the grand canonical formalism first and by use of the expression (3.4), namely

$$\begin{aligned}
&\int_0^\infty \mathrm{d}S \int_0^\infty \mathrm{d}T \int_0^\infty \mathrm{d}U' \int_0^\infty \mathrm{d}U''\, \delta(|U'-U''|-\delta)\partial_S\partial_T\partial_{U'}\partial_{U''}\mathcal{F}_{\mathrm{loop}}(S,T,U',U'';\alpha)\\
&\quad= \int_0^\infty \mathrm{d}U' \int_0^\infty \mathrm{d}U''\, \delta(|U'-U''|-\delta)\partial_{U'}\partial_{U''}\mathcal{F}_{\mathrm{loop}}(\infty,\infty,U',U'';\alpha)\\
&\quad= \int_0^\infty \mathrm{d}U' \int_0^\infty \mathrm{d}U''\, \delta(|U'-U''|-\delta)\partial_{U'}\partial_{U''}\left(\frac{3}{\alpha^2}\frac{\sinh^2(\alpha U')\sinh^2(\alpha U'')}{\sinh^2(\alpha(U'+U''))}\right)\\
&\quad= \int_0^\infty \mathrm{d}U' \int_0^\infty \mathrm{d}U''\, \delta(|U'-U''|-\delta)18\,\frac{\sinh^2(\alpha U')\sinh^2(\alpha U'')}{\sinh^4(\alpha(U'+U''))}\\
&\quad= 36\int_\delta^\infty \mathrm{d}U \frac{\sinh^2(\alpha U)\sinh^2(\alpha(U-\delta))}{\sinh^4(\alpha(2U-\delta))} = \frac{3}{2\alpha}\mathrm{e}^{-2\alpha\delta}.
\end{aligned} \tag{3.7}$$

As before, we can transform this result into the probability density for the (rescaled) variable δ in the canonical ensemble of triply pointed quadrangulations of large fixed size. This probability density reads

$$\begin{aligned}
\sigma(\delta) = \frac{2}{\mathrm{i}\sqrt{\pi}}\int_{-\infty}^{\infty}\mathrm{d}\xi\,\xi\,\mathrm{e}^{-\xi^2}\left(\frac{3}{2\alpha}\mathrm{e}^{-2\alpha\delta}\right)\Big|_{\alpha=\sqrt{-3\mathrm{i}\xi/2}} &= \sqrt{\frac{3}{\pi}}\left\{\Gamma\left(\frac{3}{4}\right){}_0F_2\left(\left\{\frac{1}{4},\frac{1}{2}\right\},-\frac{9\delta^4}{64}\right)\right.\\
&\quad -3\delta^2\Gamma\left(\frac{5}{4}\right){}_0F_2\left(\left\{\frac{3}{4},\frac{3}{2}\right\},-\frac{9\delta^4}{64}\right)\\
&\quad \left.+\sqrt{3\pi}\delta^3{}_0F_2\left(\left\{\frac{5}{4},\frac{7}{4}\right\},-\frac{9\delta^4}{64}\right)\right\},
\end{aligned} \tag{3.8}$$

where

$${}_0F_2(\{b_1,b_2\},z) \equiv \sum_{k=0}^{\infty}\frac{z^k}{k!}\frac{1}{(b_1)_k(b_2)_k}, \qquad \text{with } (b)_k \equiv \prod_{i=0}^{k-1}(b+i). \tag{3.9}$$

This probability density is plotted in figure 20. We have in particular

$$\langle\delta\rangle = \tfrac{1}{3}\langle D\rangle = 0.590\,494\ldots, \tag{3.10}$$

i.e. the common part represents on average one third of the length of a geodesic.

3.2. Confluence of minimal separating loops

The minimal separating loops themselves also exhibit a phenomenon of confluence. Indeed, a minimal separating loop is made of two geodesics of the same length emanating from a particular vertex v (with minimal label on the branch from v_1 to v_2) and reaching v_3. In the scaling limit, we expect the macroscopic minimal separating loop to be unique and moreover, its two constituent geodesics have a common part of macroscopic length δ_{loop} (see figure 21 for an illustration). Note that, although v_1, v_2 and v_3 are generic points, v is a non-typical point as it can be connected to v_3 by two distinct macroscopic geodesics which are not confluent at v. We shall call the complementary part the *open part* of the loop, with length $L'_{123} = L_{123} - 2\,\delta_{\mathrm{loop}}$.

J. Stat. Mech. (2009) P03001

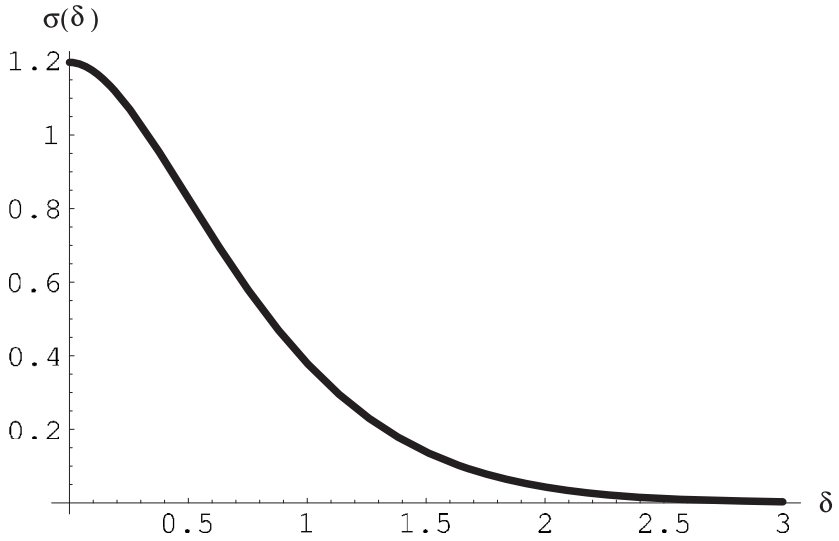

Figure 20. Plot of the probability density $\sigma(\delta)$ for the length δ of the common part of the two geodesics from v_1 and v_2 to v_3 in the scaling limit of large triply pointed quadrangulations.

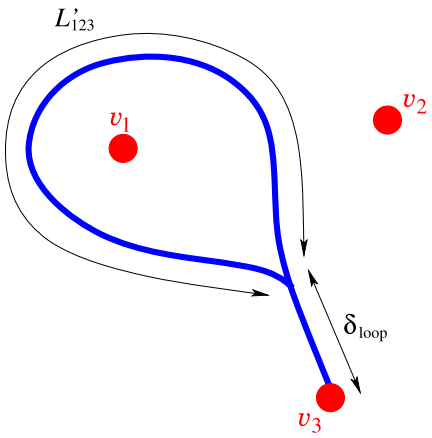

Figure 21. A schematic picture of the phenomenon of confluence of minimal separating loops. For generic points v_1, v_2 and v_3 and in the scaling limit of large quadrangulations, the minimal loop originating from v_3 and separating v_1 from v_2 (represented as a thick blue line) is unique and is made of a common part of macroscopic length $\delta_{\rm loop}$ and an open part of macroscopic length L'_{123}.

The statistics for $\delta_{\rm loop}$ and L'_{123} can be computed along the same lines as in section 3.1. In the Schaeffer approach, on the branch from v_1 to v_2 in the well-labeled tree, we now consider the vertex v with minimal label closest to v_1. Calling $1-u'$ the minimal label for trees attached the part of the branch from v_1 to v, and $1-u''$ the minimal label for trees attached to the complementary part, the quantity $|u'-u''|$ measures the length of the desired common part for a particular minimal loop formed by two chains of successors starting from v (see figure 22 for an illustration). As for the length of the open part of the loop, it is simply measured by $2\min(u',u'')$. The generating function for the objects

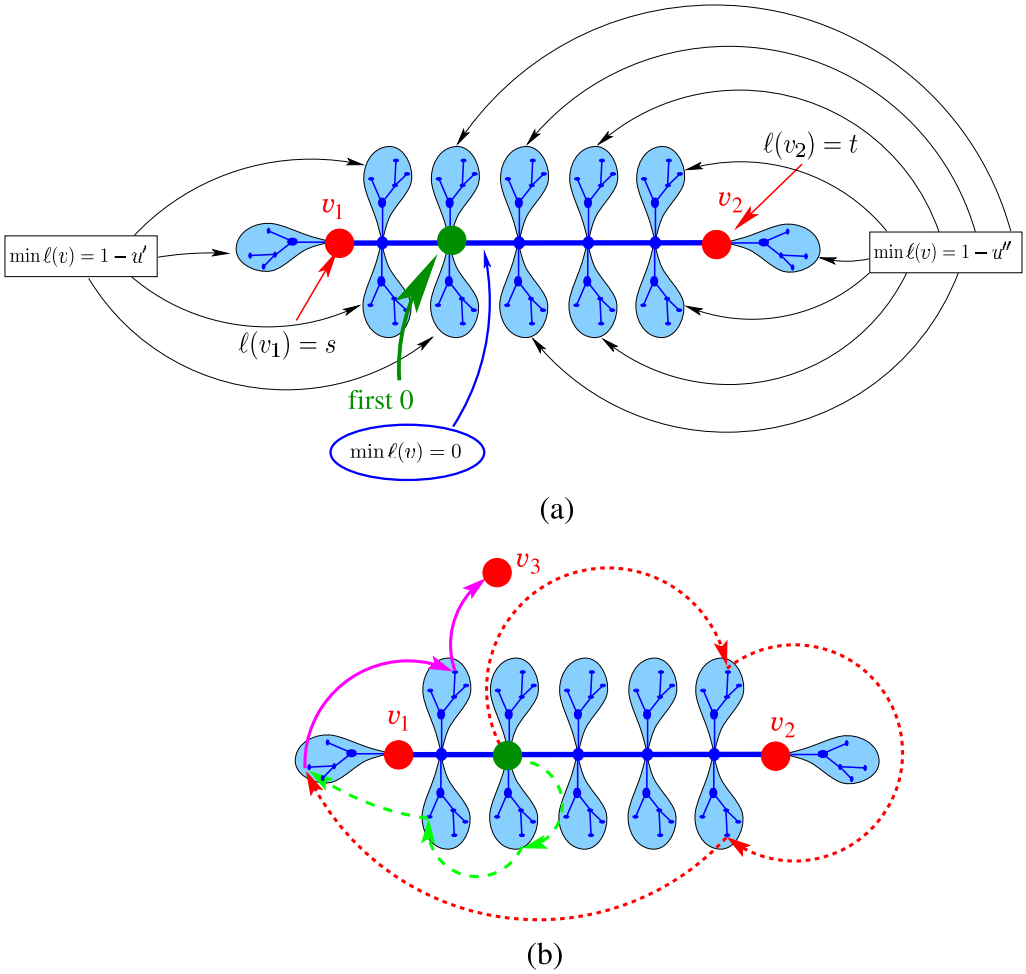

Figure 22. In the well-labeled tree of figure 5, we mark the first label 0 on the branch from v_1 to v_2 and call $1 - u'$ the minimal label on trees attached to the part of the branch lying from v_1 to the marked label 0. We also call $1 - u''$ the minimal label on trees attached to the complementary part of the branch, with $u = \max(u', u'')$. The quantity $|u' - u''|$ measures the length of the common part of a particular minimal loop originating from v_3 and separating v_1 from v_2, as apparent in (b), here in the case $u' > u''$. The length of the open part of the minimal separating loop is $2\min(u', u'') = 2u''$.

above is immediately given by

$$\Delta_{u'}\Delta_{u''}\bar{H}_{\rm loop}(s,t,u',u''), \qquad \text{where } \bar{H}_{\rm loop}(s,t,u',u'') = \tilde{X}_{s;u',u'}\, X_{u'',u''}\, \tilde{X}_{t;u'',u''}. \tag{3.11}$$

In the scaling limit, this generating function becomes

$$\partial_{U'}\partial_{U''}\bar{\mathcal{H}}_{\rm loop}(S,T,U',U'';\alpha), \qquad \text{where}$$
$$\bar{\mathcal{H}}_{\rm loop}(S,T,U',U'';\alpha) = 3\frac{\sinh^4(\alpha U')\sinh^4(\alpha U'')\sinh(\alpha(2(S+U')))\sinh(\alpha(2(T+U'')))}{\sinh(2\alpha U')\sinh(2\alpha U'')\sinh^4(\alpha(S+U'))\sinh^4(\alpha(T+U''))}, \tag{3.12}$$

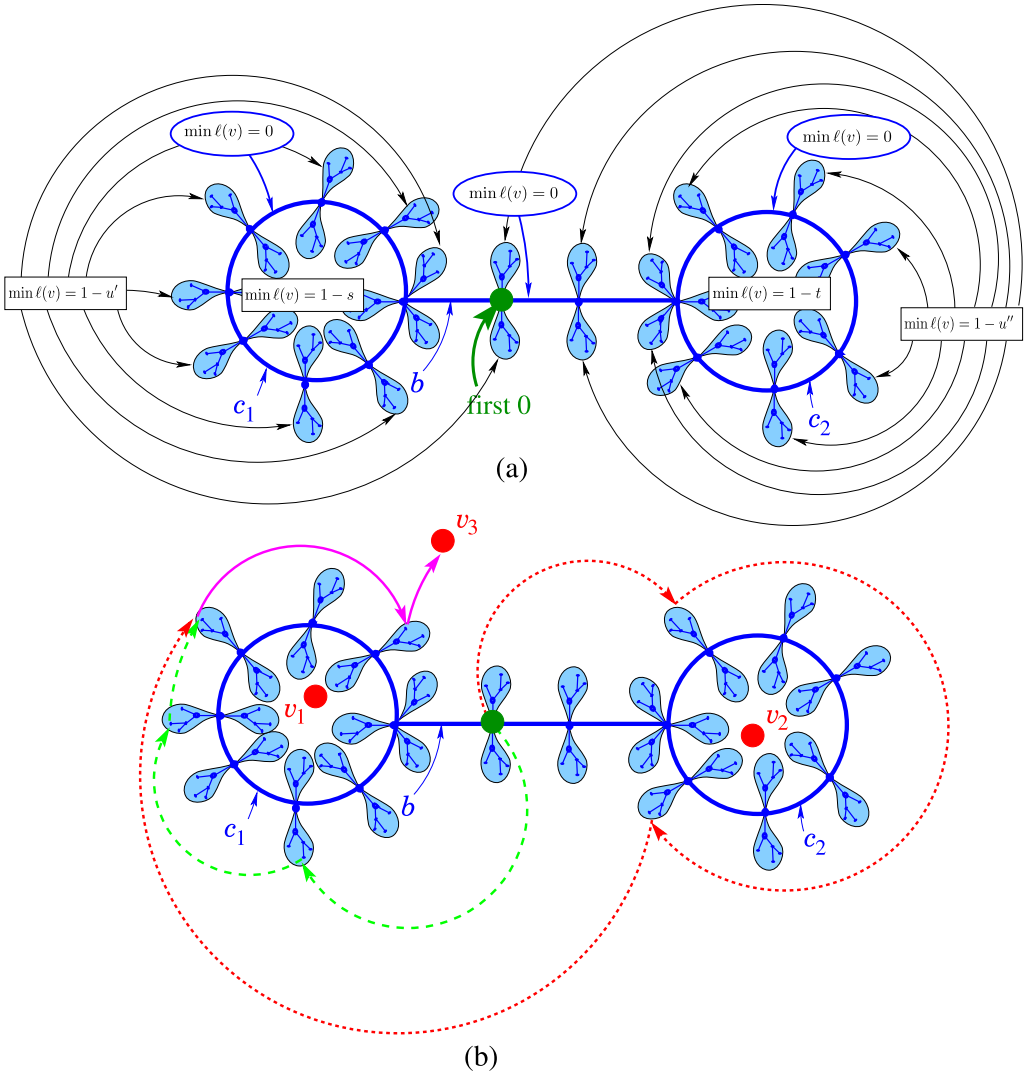

Figure 23. In the well-labeled map of figure 7, we mark the first occurrence of a label 0 on the branch b oriented from the cycle c_1 to the cycle c_2 and call $1-u'$ the minimal label on trees attached to the part of the frontier of the external face made of: (i) the part of the branch b lying between c_1 and the marked label 0 and (ii) the external side of the cycle c_1. We call $1-u''$ the minimal label on trees attached to the complementary part of the frontier, with $u = \max(u', u'')$. The quantity $|u'-u''|$ measures the length of the common part of a particular minimal loop originating for v_3 and separating v_1 from v_2, as apparent in (b), here in the case $u' > u''$ (corresponding to having the common part in the domain containing v_1). The length of the open part is $2\min(u', u'')$.

which yields the joint law for $L'_{123} = 2\min(U', U'')$, $D_{13} = S + \max(U', U'')$, $D_{23} = T + \max(U', U'')$ and $\delta_{\text{loop}} = |U' - U''|$. Note that the sign of $U' - U''$ indicates which domain delimited by the open part contains the common part of the loop. As is apparent in figure 22, this common part lies in the domain containing v_1 when $U' > U''$.

An alternative expression is found through the Miermont approach where we consider well-labeled maps of the type displayed in figure 23 using a particular minimal separating

J. Stat. Mech. (2009) P03001

loop passing through the vertex with minimal label on the branch b closest to the cycle c_1. We find a generating function

$$\begin{aligned}&\Delta_s\Delta_t\Delta_{u'}\Delta_{u''}\bar{F}_{\mathrm{loop}}(s,t,u',u''), \qquad \text{where}\\ &\bar{F}_{\mathrm{loop}}(s,t,u',u'') = X_{s,u'}\,Y_{s,u',u'}\,X_{u'',u''}\,Y_{t,u'',u''}\,X_{t,u''},\end{aligned} \tag{3.13}$$

whose scaling limit

$$\begin{aligned}&\partial_S\partial_T\partial_{U'}\partial_{U''}\bar{\mathcal{F}}_{\mathrm{loop}}(S,T,U',U'';\alpha), \qquad \text{where}\\ &\bar{\mathcal{F}}_{\mathrm{loop}}(S,T,U',U'';\alpha) =\\ &\quad\frac{3}{\alpha^2}\frac{\sinh(\alpha S)\sinh(\alpha T)\sinh^2(\alpha U')\sinh^2(\alpha U'')\sinh(\alpha(S+2U'))\sinh(\alpha(T+2U''))}{\sinh^2(\alpha(S+U'))\sinh^2(\alpha(T+U''))\sinh(2\alpha U')\sinh(2\alpha U'')}\end{aligned} \tag{3.14}$$

matches the expression (3.12) above. This matching is again a direct consequence of the identity (2.29).

We can integrate over S and T and obtain the marginal law for U' and U''

$$\frac{3}{\alpha^2}\partial_{U'}\partial_{U''}\frac{\sinh^2(\alpha U')\sinh^2(\alpha U'')}{\sinh(2\alpha U')\sinh(2\alpha U'')} = \frac{3}{4}\frac{1}{\cosh^2(\alpha U')\cosh^2(\alpha U'')}. \tag{3.15}$$

This can be translated into the marginal joint law for δ_{loop} and L'_{123}. For triply pointed quadrangulations of fixed large size n, we find the joint probability density:

$$\begin{aligned}&\tau_{\mathrm{loop}}(\delta_{\mathrm{loop}},L'_{123})\\ &\qquad=\frac{2}{\mathrm{i}\sqrt{\pi}}\int_{-\infty}^{\infty}\mathrm{d}\xi\,\xi\,\mathrm{e}^{-\xi^2}\,\frac{3/4}{\cosh^2\left(\alpha\left((L'_{123}/2)+\delta_{\mathrm{loop}}\right)\right)\cosh^2\left(\alpha(L'_{123}/2)\right)}\Bigg|_{\alpha=\sqrt{-3\mathrm{i}\xi/2}}.\end{aligned} \tag{3.16}$$

This probability density is plotted in figure 24.

Upon integrating $\tau_{\mathrm{loop}}(\delta_{\mathrm{loop}},L'_{123})$ over L'_{123}, we get the marginal density distribution for the length δ_{loop} only, namely

$$\begin{aligned}\tau_{\mathrm{loop}}(\delta_{\mathrm{loop}}) = \frac{2}{\mathrm{i}\sqrt{\pi}}\int_{-\infty}^{\infty}\mathrm{d}\xi\,\xi\,\mathrm{e}^{-\xi^2}\frac{3}{2\alpha}\frac{1}{\sinh^3(\alpha\delta_{\mathrm{loop}})\cosh(\alpha\delta_{\mathrm{loop}})}\\ \times\left\{2\cosh^2(\alpha\delta_{\mathrm{loop}})\left(\alpha\delta_{\mathrm{loop}}-\log(\cosh(\alpha\delta_{\mathrm{loop}}))\right)\right.\\ \left.-\sinh(\alpha\delta_{\mathrm{loop}})\left(\cosh(\alpha\delta_{\mathrm{loop}})+\mathrm{e}^{-\alpha\delta_{\mathrm{loop}}}\right)\right\}\Big|_{\alpha=\sqrt{-3\mathrm{i}\xi/2}}.\end{aligned} \tag{3.17}$$

This probability density is plotted in figure 25. We have in particular

$$\langle\delta_{\mathrm{loop}}\rangle = \tfrac{2}{3}(2-\log 4)\langle D\rangle = 0.724\,779\ldots \tag{3.18}$$

in terms of the average length $\langle D\rangle$ of a geodesic path.

On the other hand, upon integrating $\tau_{\mathrm{loop}}(\delta_{\mathrm{loop}},L'_{123})$ over δ_{loop}, we get the marginal density distribution for the length L'_{123} only, namely

$$\bar{\tau}_{\mathrm{loop}}(L'_{123}) = \frac{2}{\mathrm{i}\sqrt{\pi}}\int_{-\infty}^{\infty}\mathrm{d}\xi\,\xi\,\mathrm{e}^{-\xi^2}\frac{3}{4\alpha}\frac{1}{\cosh^3\left(\alpha(L'_{123}/2)\right)}\mathrm{e}^{-\alpha(L'_{123}/2)}\Bigg|_{\alpha=\sqrt{-3\mathrm{i}\xi/2}}. \tag{3.19}$$

This probability density is plotted in figure 26. We have in particular

$$\langle L'_{123}\rangle = \tfrac{4}{3}(\log 4-1)\langle D\rangle = 0.912\,418\ldots. \tag{3.20}$$

Note that $2\langle\delta_{\mathrm{loop}}\rangle+\langle L'_{123}\rangle = \frac{4}{3}\langle D\rangle$, in agreement with equation (2.34).

J. Stat. Mech. (2009) P03001

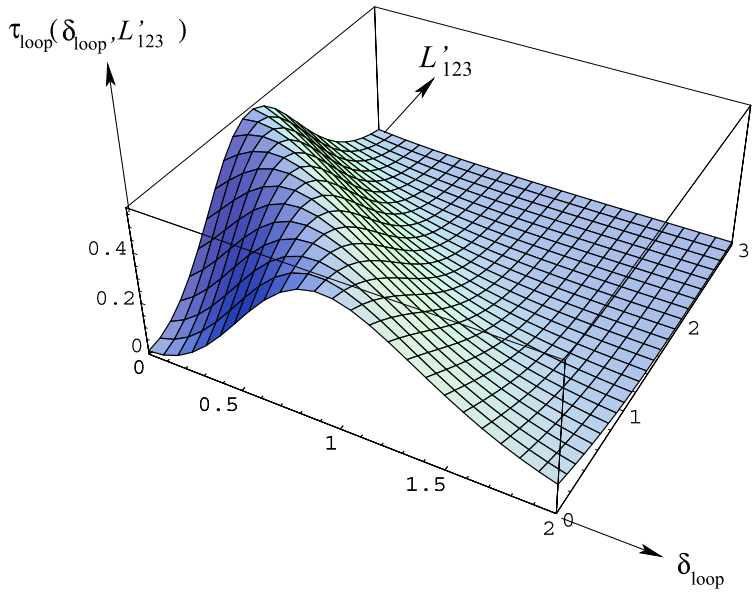

Figure 24. Plot of the joint probability density $\tau_{\rm loop}(\delta_{\rm loop}, L'_{123})$ for the length $\delta_{\rm loop}$ of the common part and the length L'_{123} of the open part of the minimal loop originating from v_3 and separating v_1 from v_2 in the scaling limit of large triply pointed quadrangulations.

3.3. Area enclosed by a minimal separating loop

Within the above framework, we may easily address the question of the partitioning of the area of triply pointed quadrangulations over the two domains separated by a minimal separating loop. For a given separating loop, we may indeed decide to attach a weight per face of the quadrangulation depending on which domain it lies in. In the equivalent Miermont picture and for the particular minimal separating loop considered in figure 23, this amounts to assigning a weight, say g_1 (respectively g_2), to edges lying in the domain containing v_1 (respectively v_2), which results in the generating function

$$\Delta_s\Delta_t\Delta_{u'}\Delta_{u''}\bar{F}_{\rm loop}(s,t,u',u'';g_1,g_2), \qquad \text{where}$$
$$\bar{F}_{\rm loop}(s,t,u',u'';g_1,g_2) = X_{s,u'}(g_1)\,Y_{s,u',u'}(g_1)\,X_{u'',u''}(g_2)\,Y_{t,u'',u''}(g_2)\,X_{t,u''}(g_2). \tag{3.21}$$

Here $X_{s,t}(g_m)$ and $Y_{s,t,u}(g_m)$ denote the generating functions $X_{s,t}$ and $Y_{s,t,u}$, as given by (2.13) and (2.15), with g replaced by g_m in (2.12), for $m = 1, 2$. In the continuum limit, we set

$$g_1 = \tfrac{1}{12}(1-\Lambda_1\epsilon), \qquad g_2 = \tfrac{1}{12}(1-\Lambda_2\epsilon), \tag{3.22}$$

which amounts to having different cosmological constants in the two domains. The generating function above translates into the scaling function

$$\partial_S\partial_T\partial_{U'}\partial_{U''}\bar{\mathcal{F}}_{\rm loop}(S,T,U',U'';\alpha_1,\alpha_2), \qquad \text{where}$$
$$\bar{\mathcal{F}}_{\rm loop}(S,T,U',U'';\alpha_1,\alpha_2) = 3^3\mathcal{Y}(S,U',U';\alpha_1)\mathcal{Y}(T,U'',U'';\alpha_2),$$
$$\mathcal{Y}(S,T,U;\alpha) \equiv \frac{1}{3\alpha}\frac{\sinh(\alpha S)\sinh(\alpha T)\sinh(\alpha U)\sinh(\alpha(S+T+U))}{\sinh(\alpha(S+T))\sinh(\alpha(T+U))\sinh(\alpha(U+S))}, \tag{3.23}$$

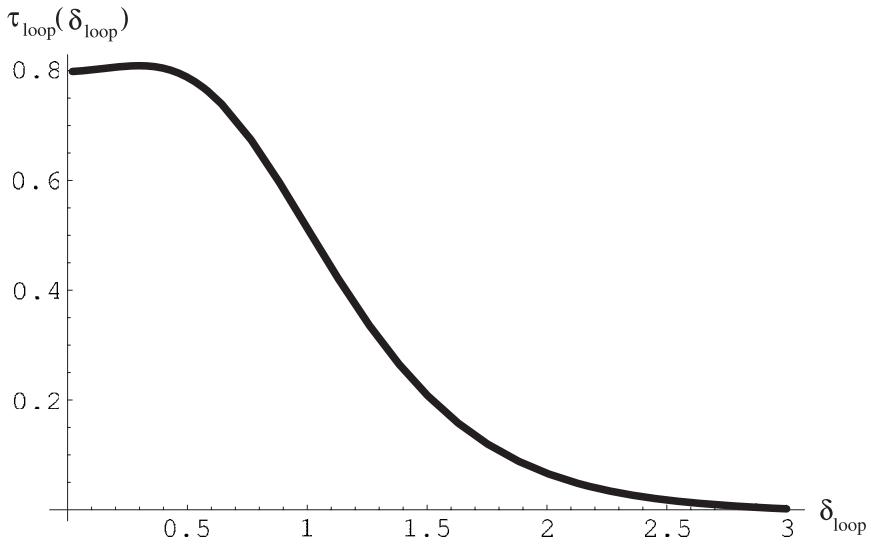

Figure 25. Plot of the marginal probability density $\tau_{\mathrm{loop}}(\delta_{\mathrm{loop}})$ for the length of the common part of the minimal loop originating from v_3 and separating v_1 from v_2 in the scaling limit of large triply pointed quadrangulations.

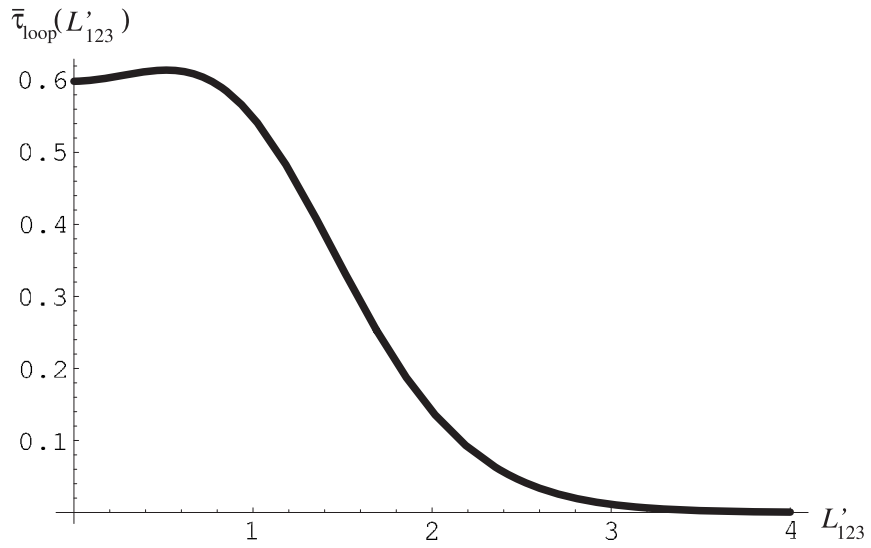

Figure 26. Plot of the marginal probability density $\bar{\tau}_{\mathrm{loop}}(L'_{123})$ for the length of the open part of the minimal loop originating from v_3 and separating v_1 from v_2 in the scaling limit of large triply pointed quadrangulations.

and $\alpha_m = \sqrt{3/2}\Lambda_m^{1/4}$. Here, $\mathcal{Y}$ is the scaling limit of Y, while each X tends to 3 in the scaling limit, irrespectively of its arguments.

Upon integrating over all possible values of S, T, U' and U'', we get a function

$$\bar{\mathcal{F}}_{\mathrm{loop}}(\infty,\infty,\infty,\infty;\alpha_1,\alpha_2) = \frac{3}{4\alpha_1\alpha_2}. \tag{3.24}$$

Returning to the canonical formalism where we fix the sizes of the two domains separated by the minimal loop to be respectively n_1 and n_2 (with $n_1+n_2=n$, $n_1\gg 1$, $n_2\gg 1$), we set $\epsilon=1/n$ and $\Lambda_m=-\xi_m^2$, so that the expression (3.24) tends to $n^{1/2}\mathrm{i}/(2\sqrt{\xi_1\xi_2})$. Setting $n_1=\eta n$ and $n_2=(1-\eta)n$, we obtain the probability density for η as

$$\begin{aligned}\varrho(\eta)&=\frac{2}{\mathrm{i}\pi^{3/2}}\int_{-\infty}^{\infty}\mathrm{d}\xi_1\,\xi_1\mathrm{e}^{-\eta\xi_1^2}\int_{-\infty}^{\infty}\mathrm{d}\xi_2\,\xi_2\mathrm{e}^{-(1-\eta)\xi_2^2}\frac{1}{2\sqrt{\xi_1\xi_2}}\\&=\frac{\sqrt{\pi}}{\Gamma\left(\frac{1}{4}\right)}\frac{1}{\eta^{3/4}(1-\eta)^{3/4}}.\end{aligned}\tag{3.25}$$

The partitioning η of the mass is therefore governed by a simple Beta distribution with parameters $\{1/4,1/4\}$. In particular the two domains are most likely of very asymmetric sizes, with a probability density maximal for $\eta=0$ or 1.

More precisely, we can naturally distinguish the two domains as exactly one of them contains the common part of the minimal separating loop. As mentioned above, this information is encoded in the sign of $U'-U''$. We may integrate (3.23) over S, T, U' and U'' in the domain $U'>U''$, corresponding to the case where the common part lies in the domain containing v_1. This leads to

$$\int_0^{\infty}\mathrm{d}U'\,\frac{3}{4\alpha_1\alpha_2}\left[\partial_{U'}\tanh(\alpha_1U')\right]\tanh(\alpha_2U'),\tag{3.26}$$

which, together with the symmetric contribution from the domain $U''>U'$ (obtained by exchanging α_1 and α_2), adds up to (3.24). We can in principle deduce from (3.26) the (now asymmetric) law for η conditionally on the position of the common part. We have not found a compact simple form for this law but its first few moments can be computed. We find an average value

$$\langle\eta\rangle_{U'>U''}=\langle 1-\eta\rangle_{U''>U'}=\tfrac{1}{3}(1+\log 4)\sim 79.543\%\tag{3.27}$$

for the proportion of the total area lying in the same domain as the common part of the minimal separating loop.

4. The three-point function revisited

The three-point function of planar quadrangulations enumerates quadrangulations of the sphere with three marked vertices v_1, v_2 and v_3 *at prescribed pairwise distances* d_{12}, d_{23} and d_{31}. It was computed in [15] and, in the scaling limit of quadrangulations of fixed large size $n\to\infty$, translates into a universal joint probability $\rho(D_{12},D_{23},D_{31})$ for the three rescaled lengths $D_{12}=d_{12}/n^{1/4}$, $D_{23}=d_{23}/n^{1/4}$ and $D_{31}=d_{31}/n^{1/4}$ of the three geodesics forming the triangle (v_1,v_2,v_3). As mentioned in section 1, a full description of the geometry of this triangle must incorporate the phenomenon of confluence. We call the lengths of the common parts respectively δ_1 (for the two geodesics leading to v_1), δ_2 (for the two geodesics leading to v_2) and δ_3 (for the two geodesics leading to v_3). The remaining proper parts of the geodesics form an open triangle with sides of respective lengths $D'_{12}=D_{12}-\delta_1-\delta_2$, $D'_{23}=D_{23}-\delta_2-\delta_3$ and $D'_{31}=D_{31}-\delta_3-\delta_1$ (see figure 27 for an illustration). A natural question is that of determining the corresponding joint probability density $\rho(D'_{12},D'_{23},D'_{31},\delta_1,\delta_2,\delta_3)$.

J. Stat. Mech. (2009) P03001

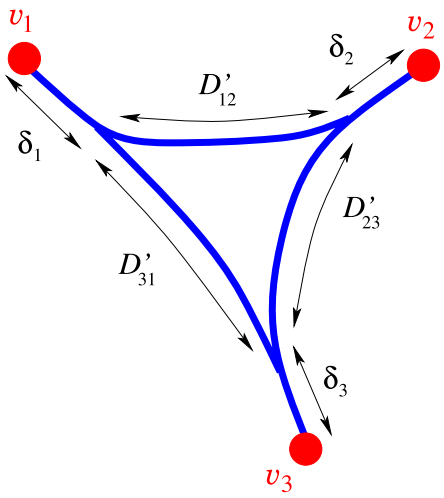

Figure 27. A schematic picture of the phenomenon of confluence of geodesics for the three geodesics linking three generic points v_1, v_2 and v_3 in the scaling limit of large quadrangulations. These geodesics (represented as thick blue lines) have common parts of macroscopic lengths δ_1, δ_2 and δ_3. The remaining open part of the triangle has sides of macroscopic lengths D'_{12}, D'_{23} and D'_{31}, and separates the quadrangulation into two domains. The three common parts may lie in the same domain (as represented here) or in different domains, giving rise to eight possibilities for the relative position of the three geodesics (see figure 33 below).

As explained in [15], triply pointed quadrangulations with prescribed values of the pairwise distances d_{12}, d_{23} and d_{31} are in one-to-one correspondence with particular well-labeled maps with three faces. This is again a consequence of the Miermont bijection with three sources v_1, v_2 and v_3, and with a particular choice of delays, now given by

$$\tau_1 = -s \equiv \frac{d_{23} - d_{31} - d_{12}}{2}, \qquad \tau_2 = -t \equiv \frac{d_{31} - d_{12} - d_{23}}{2}, \qquad \tau_3 = -u \equiv \frac{d_{12} - d_{23} - d_{31}}{2}, \tag{4.1}$$

where we use the parameterization of the pairwise distances

$$d_{12} = s + t, \qquad d_{23} = t + u, \qquad d_{31} = u + s. \tag{4.2}$$

As shown in [15], the maps obtained for this choice of delays are now of the type displayed in figure 28, or degenerate versions of this generic form when one of the frontiers between faces or one of the faces reduces to a single vertex. By an simple decomposition of the map in five pieces obtained by cutting the map at the first and last occurrences of a label 0 on each frontier, we immediately get the generating function for these maps:

$$\Delta_s \Delta_t \Delta_u F(s,t,u), \qquad \text{where } F(s,t,u) = X_{s,t}\, X_{t,u}\, X_{u,s}\, (Y_{s,t,u})^2. \tag{4.3}$$

If we now consider, say, the first label 0 on each of the three pairwise frontiers between faces, the global frontier of each face can then be divided into two parts lying in between the two marked labels 0 on this frontier. We may then distinguish the minimal label on trees attached to the first part of the frontier from that on trees attached to the second

J. Stat. Mech. (2009) P03001

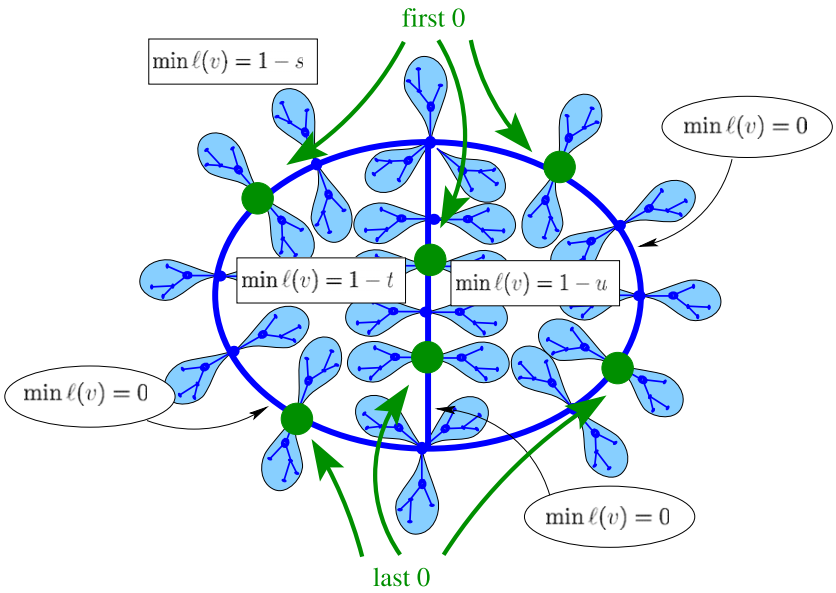

Figure 28. Structure of the well-labeled maps with three faces coding triply pointed quadrangulations with prescribed values of the pairwise distances between the marked vertices: $d_{12} = s + t$, $d_{23} = t + u$ and $d_{31} = u + s$. These maps are easily enumerated by cutting them at the first and last labels 0 on each frontier (big green dots).

part of the frontier (see figure 29(a) for an illustration). For instance, the minimal label $1 - s$ in the first face corresponds to a minimal label $1 - s'$ on one part and $1 - s''$ on the other part with $s = \max(s', s'')$. We have similar minima $1-t'$, $1-t''$ and $1-u'$, $1-u''$ in the other faces. The quantities $|s' - s''|$, $|t' - t''|$ and $|u' - u''|$ measure the lengths of the pairwise common parts of three particular geodesics made of chains of successors of corners at the marked labels 0 (see figure 29(b)). Similarly, the quantities $\min(s', s'') + \min(t', t'')$, $\min(t', t'') + \min(u', u'')$ and $\min(u', u'') + \min(s', s'')$ are the lengths of the proper parts of the same three geodesics. With the above refinements, the generating function now reads

$$\begin{aligned} &\Delta_{s'}\Delta_{s''}\Delta_{t'}\Delta_{t''}\Delta_{u'}\Delta_{u''}F(s', s'', t', t'', u', u''), \qquad \text{where} \\ &F(s', s'', t', t'', u', u'') = X_{s'',t''}\, X_{t'',u''}\, X_{u'',s''}\, Y_{s',t',u'}\, Y_{s'',t'',u''}, \end{aligned} \tag{4.4}$$

and its continuous counterpart reads

$$\begin{aligned} &\partial_{S'}\partial_{S''}\partial_{T'}\partial_{T''}\partial_{U'}\partial_{U''}\mathcal{F}(S', S'', T', T'', U', U''; \alpha), \qquad \text{where} \\ &\mathcal{F}(S', S'', T', T'', U', U''; \alpha) = 3^3\mathcal{Y}(S', T', U'; \alpha)\mathcal{Y}(S'', T'', U''; \alpha), \\ &\mathcal{Y}(S, T, U; \alpha) = \frac{1}{3\alpha}\frac{\sinh(\alpha S)\sinh(\alpha T)\sinh(\alpha U)\sinh(\alpha(S+T+U))}{\sinh(\alpha(S+T))\sinh(\alpha(T+U))\sinh(\alpha(U+S))}, \end{aligned} \tag{4.5}$$

which yields directly the joint law $\rho(D'_{12}, D'_{23}, D'_{31}, \delta_1, \delta_2, \delta_3)$ for $D'_{12} = \min(S', S'') + \min(T', T'')$, $D'_{23} = \min(T', T'') + \min(U', U'')$, $D_{31} = \min(U', U'') + \min(S', S'')$, $\delta_1 = |S' - S''|$, $\delta_2 = |T' - T''|$ and $\delta_3 = |U' - U''|$. Note that the sign of $S' - S''$ (respectively $T' - T''$, $U' - U''$) indicates in which of the domains delimited by the open part of the

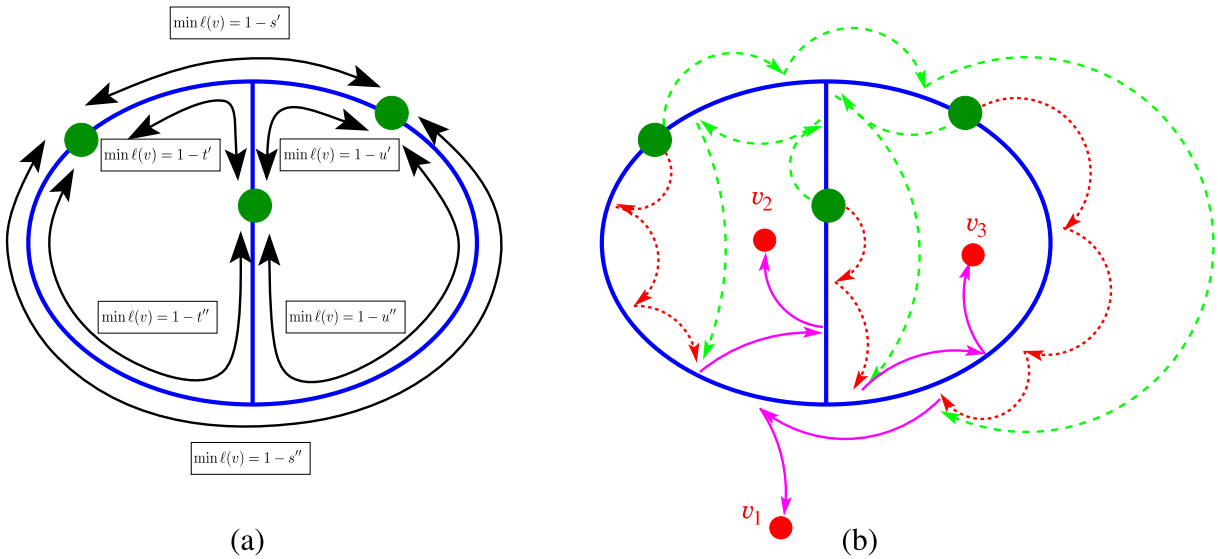

Figure 29. In the map of figure 28, we mark the first label 0 on each frontier. We then call $1-s'$, $1-s''$, $1-t'$, $1-t''$, $1-u'$ and $1-u''$ respectively the minimal labels on trees attached to the six frontier sides delimited by these marked points as shown, with $s=\max(s',s'')$, $t=\max(t',t'')$ and $u=\max(u',u'')$. The quantities $|s'-s''|$, $|t'-t''|$ and $|u'-u'|$ measure the lengths of the common parts (represented by solid magenta arrows) of three particular geodesics obtained from the concatenation of chains of successors of the marked labels 0. The situation represented here corresponds to $s''>s'$, $t''>t'$ and $u''>u'$.

triangle the common part leading to v_1 (respectively v_2, v_3) lies. Let us now discuss in more detail a number of marginal laws inherited from $\rho(D'_{12},D'_{23},D'_{31},\delta_1,\delta_2,\delta_3)$.

A first marginal law is that for the lengths δ_1, D'_{12} and δ_2 of the three parts of the geodesic between v_1 and v_2. It is obtained by first integrating (4.5) over U' and U'', which yields $\partial_{S'}\partial_{S''}\partial_{T'}\partial_{T''}\mathcal{F}(S',S'',T',T'',\infty,\infty)$, then integrating over S', S'', T' and T'' with fixed values $\min(S',S'')=\sigma$, $\max(S',S'')=\sigma+\delta_1$, $\min(S',S'')=\tau$, $\max(S',S'')=\tau+\delta_2$, and finally integrating over σ and τ with the condition $\sigma+\tau=D'_{12}$. We obtain the grand canonical function

$$\begin{aligned}\frac{3}{2}\alpha\left\{\frac{1}{\sinh^3(\alpha D'_{12})\sinh^3(\alpha(D'_{12}+\delta_1+\delta_2))}+\frac{1}{\sinh^3(\alpha(D'_{12}+\delta_1))\sinh^3(\alpha(D'_{12}+\delta_2))}\right\}\\ \times\{2\alpha D'_{12}(2\cosh(\alpha\delta_1)\cosh(\alpha\delta_2)+\cosh(\alpha(2D'_{12}+\delta_1+\delta_2)))\\ +2\sinh(\alpha(\delta_1+\delta_2))-2\sinh(\alpha(2D'_{12}+\delta_1+\delta_2))\\ -\cosh(\alpha(\delta_1-\delta_2))\sinh(2\alpha D'_{12})\},\end{aligned}\tag{4.6}$$

from which we can get the canonical joint probability density $\theta(\delta_1,\delta_2,D'_{12})$ as before. It is interesting to consider this probability density conditionally on the value of the total length D_{12} of the geodesic between v_1 and v_2, namely

$$\theta(\delta_1,\delta_2|D_{12})=\frac{\theta(\delta_1,\delta_2,D_{12}-\delta_1-\delta_2)}{\rho(D_{12})},\tag{4.7}$$

J. Stat. Mech. (2009) P03001

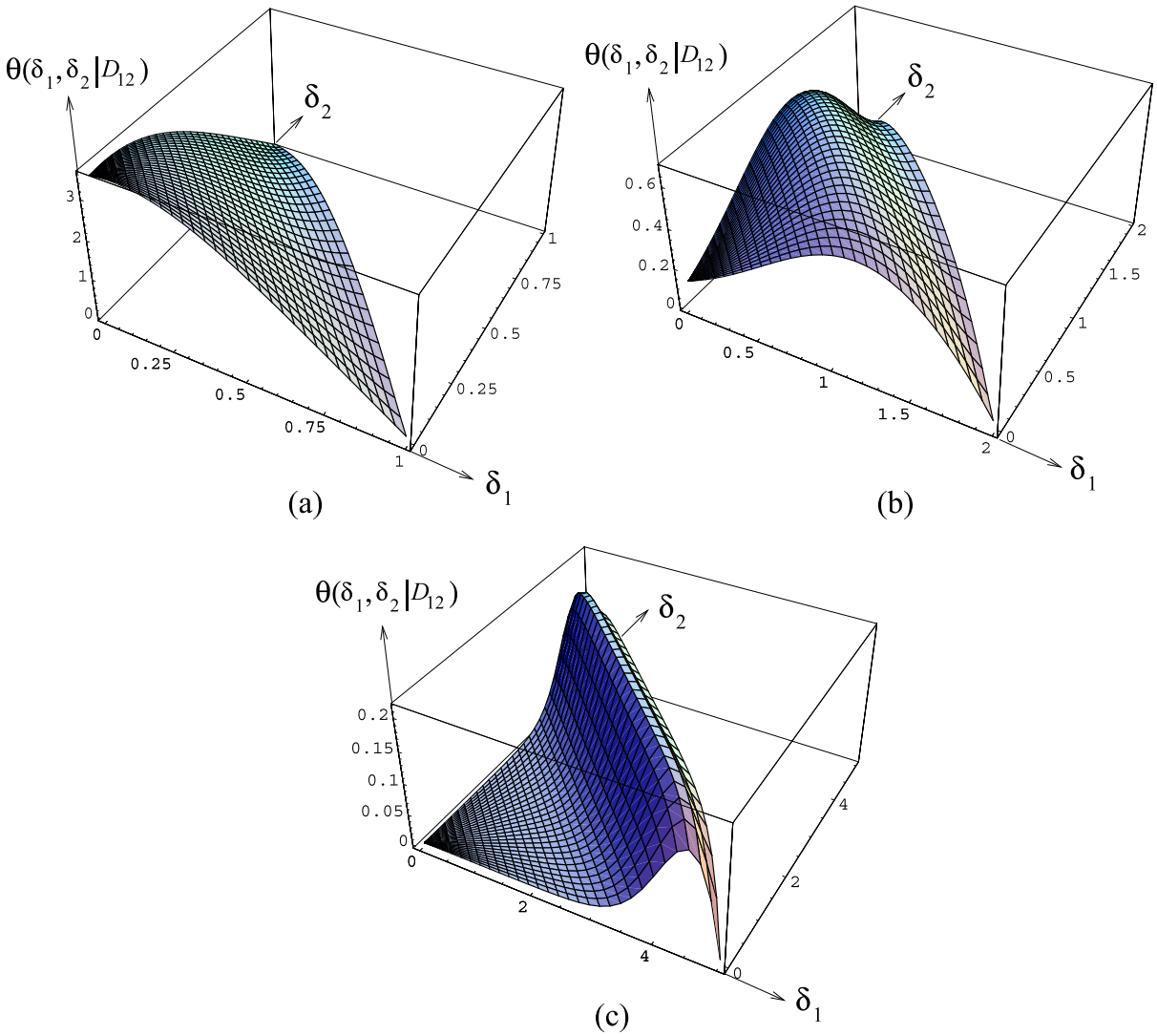

Figure 30. Plots of the conditional probability density $\theta(\delta_1, \delta_2|D_{12})$ for the lengths of the two common parts of a geodesic of fixed length D_{12}, here for (a) $D_{12} = 1.0$, (b) 2.0 and (c) 5.0.

where $\rho(D)$ is the canonical two-point function (2.39). This conditional probability density is plotted in figure 30 for $D_{12} = 1.0$, 2.0 and 5.0.

At large D_{12}, it takes the simple form

$$\theta(\delta_1, \delta_2|D_{12}) \sim \frac{1}{D_{12}} \times (9D_{12})^{1/3} \chi((9D_{12})^{1/3}(D_{12} - \delta_1 - \delta_2)),$$
$$\text{where } \chi(\lambda) = \frac{1}{3}\left(\frac{1}{\sinh^3(\lambda/2)} + \frac{8}{\mathrm{e}^{3\lambda/2}}\right)(\lambda\cosh(\lambda/2) - 2\sinh(\lambda/2)). \tag{4.8}$$

In this limit, the geodesic consists mainly of two common parts linked by a small open part whose length is of order $D_{12}^{-1/3}$, with a distribution given by the scaling function $\chi(\lambda)$.

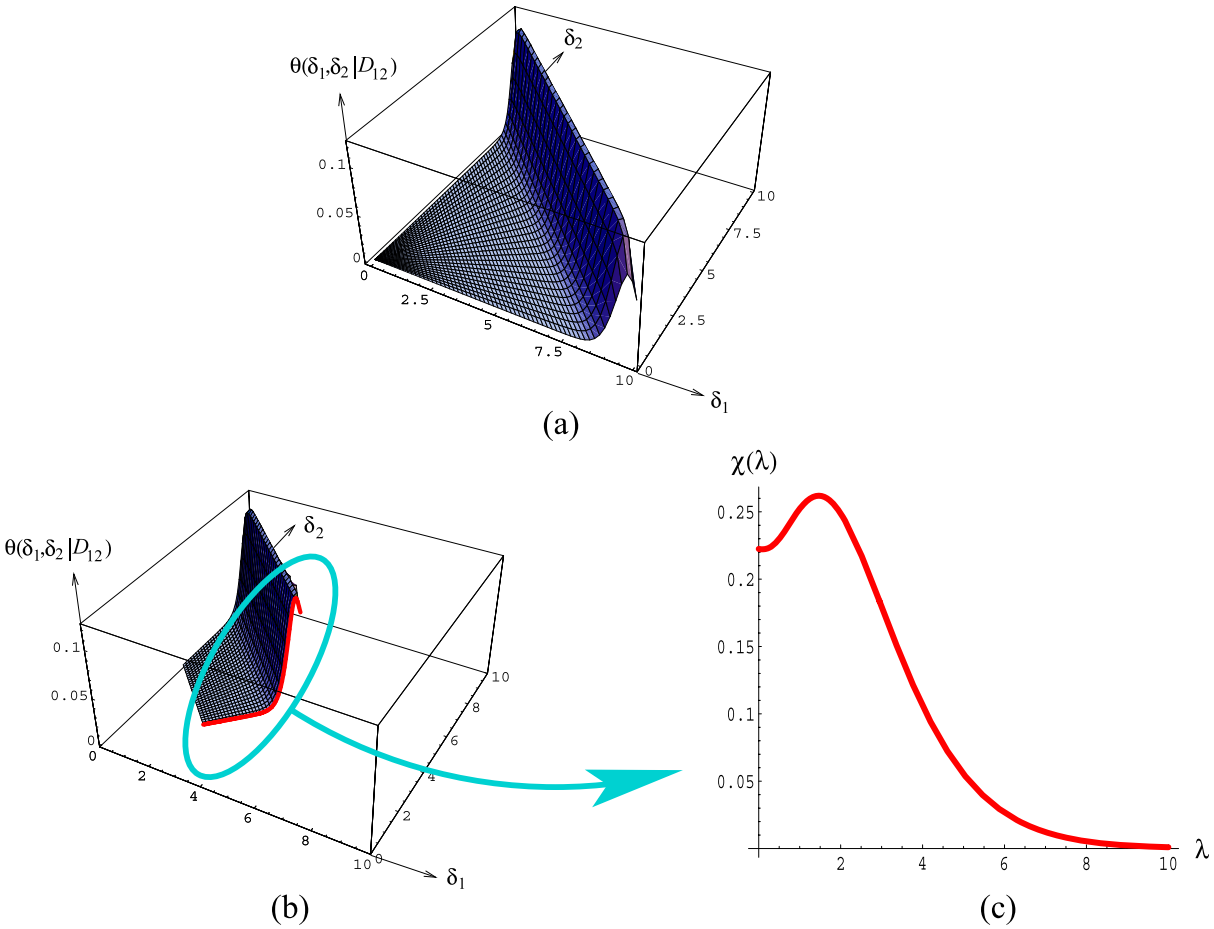

Figure 31. The conditional probability density $\theta(\delta_1, \delta_2|D_{12})$ for a large value of D_{12} (here $D_{12} = 10.0$) becomes uniform in the 'transverse' direction (corresponding to fixing the value of $\delta_1 + \delta_2$) and characterized by the scaling function $\chi(\lambda)$ in the 'longitudinal' direction (corresponding to varying the value of $\delta_1 + \delta_2$), with a scaling variable $\lambda = (9D_{12})^{1/3} D'_{12} = (9D_{12})^{1/3}(D_{12} - \delta_1 - \delta_2)$.

The position of this open part is moreover uniform along the geodesic. This property is illustrated in figure 31.

Upon integrating (4.6) over δ_1 and δ_2, we can get the marginal law for D'_{12} only. In the grand canonical formalism, it reads

$$\frac{3}{16\alpha \sinh^4(\alpha D'_{12})}\{2\alpha D'_{12}(8 + 13\mathrm{e}^{-2\alpha D'_{12}} - 4\mathrm{e}^{-4\alpha D'_{12}} + \mathrm{e}^{-6\alpha D'_{12}}) - (1 - \mathrm{e}^{-2\alpha D'_{12}})(20 - 3\mathrm{e}^{-2\alpha D'_{12}} + \mathrm{e}^{-4\alpha D'_{12}})\}, \tag{4.9}$$

from which we obtain the canonical probability density $\theta(D'_{12})$. This probability density is plotted in figure 32. We have in particular

$$\langle D'_{12} \rangle = \tfrac{1}{3} \langle D \rangle = 0.590\,494\ldots, \tag{4.10}$$

i.e. the length of the open part represents on average one third of the length of a geodesic, in agreement with (3.10). Upon integrating (4.6) over D'_{12} and δ_2 and turning to the

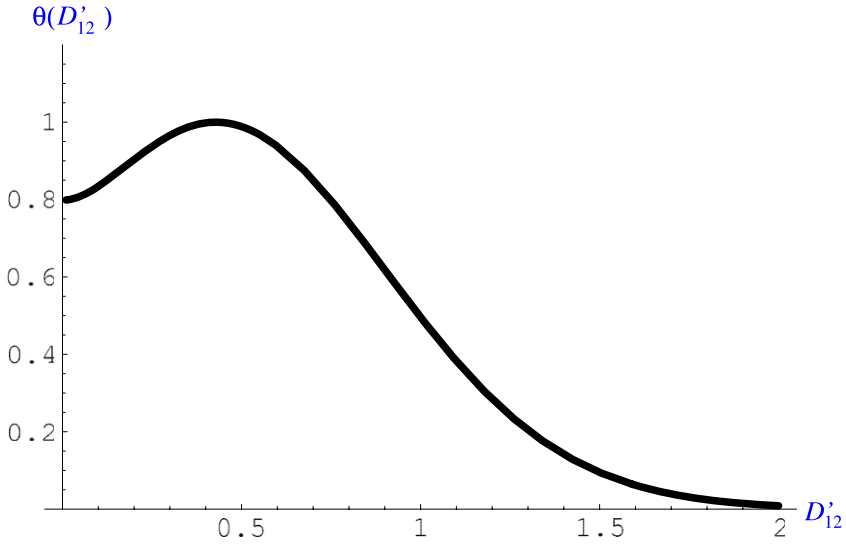

Figure 32. Plot of the probability density $\theta(D'_{12})$ for the length D'_{12} of the proper part of the geodesic between v_1 and v_2 in the scaling limit of large triply pointed quadrangulations.

canonical formalism, we can recover the marginal law $\sigma(\delta_1)$ of section 3.1. Similarly, upon integrating (4.6) over D'_{12}, δ_1 and δ_2 with a fixed value of $D_{12} = D'_{12} + \delta_1 + \delta_2$, and upon turning to the canonical formalism, we recover the two-point function $\rho(D_{12})$, as we should.

To conclude this section, let us finally discuss the global arrangement of the three geodesics on the sphere. As illustrated in figure 33, there are eight possibilities: in two cases ((a) and (h) in figure 33), the three common parts lie in the same domain, while in the remaining six cases ((b)–(g) in figure 33), two of the common parts lie in the same domain and the third one in the other domain.

We may wonder what the probability is of observing a given arrangement in the canonical ensemble. Any of the above arrangements corresponds simply to a choice of sign for $S' - S''$, $T' - T''$ and $U' - U''$. To obtain, say, arrangement (a), we may integrate (4.5) with the conditions $S' = \max(S', S'') = S$, $T' = \max(T', T'') = T$, $U' = \max(U', U'') = U$, leading to the grand canonical function

$$3^3 \left(\partial_S \partial_T \partial_U \mathcal{Y}(S, T, U; \alpha)\right) \mathcal{Y}(S, T, U; \alpha). \tag{4.11}$$

To obtain arrangement (b), the third condition must be replaced by $U'' = \max(U', U'') = U$, leading to a grand canonical function

$$3^3 \left(\partial_S \partial_T \mathcal{Y}(S, T, U; \alpha)\right) \left(\partial_U \mathcal{Y}(S, T, U; \alpha)\right). \tag{4.12}$$

All the remaining arrangements follow by symmetry and their contributions add up to the grand canonical three-point function

$$3^3 \partial_S \partial_T \partial_U \left(\mathcal{Y}(S, T, U; \alpha)\right)^2, \tag{4.13}$$

which is the continuous limit of equation (4.3). To obtain the probability of having a given arrangement, we simply have to integrate its individual contribution over S, T, U, and

J. Stat. Mech. (2009) P03001

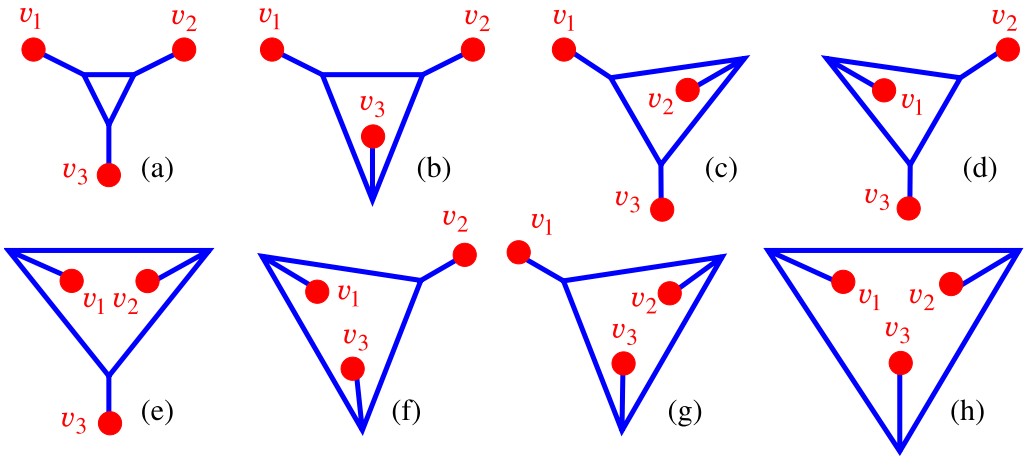

Figure 33. A schematic picture of the eight possible arrangements for the three common parts of the geodesics with respect to their open part. In the cases (a) and (h), the three common parts lie on the same side of the open part. In the remaining cases, two of the common parts lie on the same side and the third one on the other side. Note that, due to the orientation of the sphere, (a) and (h) (respectively (b) and (e), (c) and (f), (d) and (g)) can be distinguished through the cyclic order of the three sources.

divide by the integral of (4.13). Note that this ratio, obtained in the grand canonical ensemble, yields directly the correct canonical probability since all grand canonical individual contributions integrate to a numerical constant times the same function $1/\alpha^2$. A simple calculation shows that each of the arrangements (a) and (h) occurs with a probability 1/4, while each of the arrangements (b)–(g) occurs with a probability 1/12.

As for the partitioning of the area over the two domains, we find that, if we disregard the particular arrangement at hand, the probability density for the proportion η of the total area lying in one of the two domains is again given by the symmetric Beta distribution (3.25) with parameters $\{1/4, 1/4\}$. On the other hand, if we consider a particular arrangement, the partitioning of the area is no longer symmetric over the two domains. In the case of arrangement (a) or (h), we find that, on average, ∼94.259% of the total area lies in the domain containing the three common parts, while, in the case of the arrangement (b), (c), (d), (e), (f) or (g), an average of ∼67.224% of the total area lies in the domain containing the two common parts.

5. Conclusion and discussion

In this paper, we derived a number of probability distributions for the lengths and areas of triangles made of the three geodesics connecting three uniformly drawn random points, as well as of minimal separating loops. These laws are expected to be universal features of the Brownian map and provide quantitative results characterizing the phenomenon of confluence. This phenomenon is remarkable as it places the Brownian map halfway between smooth surfaces and trees. In smooth surfaces, geodesics cannot merge and the three sides of a triangle only meet at their end-points, so there are no common parts. In contrast, in trees, the three sides of a triangle meet at a central common vertex, so there

J. Stat. Mech. (2009) P03001

is no open part. As for a minimal separating loop on a tree, it corresponds generically to a back-and-forth travel to the above central common vertex and hence has no open part. On a smooth surface, depending on the shape of the surface, a minimal separating loop is either a back-and-forth travel along a geodesic, with no open part, or a simple curve with no common part. Having both open and common parts of non-zero length is a peculiarity of the Brownian map.

It is tempting to relate the above results to the so-called 'baby universe structure' of two-dimensional quantum gravity well-known in the physics literature [3, 22]. In this picture, a baby universe is a region of the surface separated by a small neck, and a typical surface consists of many such baby universes attached to a mother universe and arranged in a tree-like fashion. The influence of baby universes on the behavior of the three-point function was already discussed in [16]. Qualitatively, the confluence phenomenon could simply result from the fact that a typical point lies in a baby universe and all geodesics leading to it are forced to pass through the same chain of small necks. The length of the common part of geodesics could then be interpreted as a measure of the spatial extent of baby universes. More precise statements would require a rigorous definition of baby universes at a discrete level. A first possibility consists in looking only at so-called 'minimum neck baby universes' (*minbus*) [22]. It was shown however that a typical minbu remains finite [23], and hence its extent vanishes in the continuum limit. One should then look at more general baby universes with larger necks but one then faces the problem that there is no canonical decomposition of a general map in such baby universes.

Our approach consisted in obtaining discrete results for random quadrangulations and taking their scaling limit. So far we lack a general formalism which would allow us to compute the same results directly in the continuum. Despite recent progress [24, 25], the so-called Liouville field theory does not yet seem to be able to address such questions. Moreover, our results are restricted to the so-called universality class of pure gravity. It would be desirable to extend them to other universality classes of random surfaces coupled to critical matter models [2] (characterized by their central charge c, the pure gravity having $c = 0$) such as the celebrated Ising model ($c = 1/2$) [26]. Discrete approaches based on bijections with blossom trees [27]–[29] or labeled trees [30, 31] exist for these problems but those have not been used, so far, to extract geometrical information. Some of these models (with a central charge $c > 1$) are expected to behave like branched polymers, and hence should have the geometry of trees described above.

References

[1] Kazakov V, *Bilocal regularization of models of random surfaces*, 1985 *Phys. Lett.* B **150** 282
David F, *Planar diagrams, two-dimensional lattice gravity and surface models*, 1985 *Nucl. Phys.* B **257** 45
Ambjørn J, Durhuus B and Fröhlich J, *Diseases of triangulated random surface models and possible cures*, 1985 *Nucl. Phys.* B **257** 433
Kazakov V, Kostov I and Migdal A, *Critical properties of randomly triangulated planar random surfaces*, 1985 *Phys. Lett.* B **157** 295

[2] For a review, see: Di Francesco P, Ginsparg P and Zinn-Justin J, *2D gravity and random matrices*, 1995 *Phys. Rep.* **254** 1

[3] Ambjørn J, Durhuus B and Jonsson T, 1997 *Quantum Geometry: A Statistical Field Theory Approach* (Cambridge: Cambridge University Press)

[4] Marckert J F and Mokkadem A, *Limit of normalized quadrangulations: the Brownian map*, 2006 *Ann. Probab.* **34** 2144 [arXiv:math.PR/0403398]

[5] Le Gall J F, *The topological structure of scaling limits of large planar maps*, 2007 *Invent. Math.* **169** 621 [arXiv:math.PR/0607567]

J. Stat. Mech. (2009) P03001

[6] Le Gall J F and Paulin F, *Scaling limits of bipartite planar maps are homeomorphic to the 2-sphere*, 2006 arXiv:math.PR/0612315

[7] Miermont G, *On the sphericity of scaling limits of random planar quadrangulations*, 2008 *Electron. Commun. Probab.* **13** 248 arXiv:0712.3687 [math.PR]

[8] Ambjørn J and Watabiki Y, *Scaling in quantum gravity*, 1995 *Nucl. Phys.* B **445** 129

[9] Bouttier J, Di Francesco P and Guitter E, *Geodesic distance in planar graphs*, 2003 *Nucl. Phys.* B **663** 535 [arXiv:cond-mat/0303272]

[10] Chassaing P and Schaeffer G, *Random planar lattices and integrated superBrownian excursion*, 2004 *Probab. Theory Relat. Fields* **128** 161 [arXiv:math.CO/0205226]

[11] Miermont G and Weill M, *Radius and profile of random planar maps with faces of arbitrary degrees*, 2008 *Electron. J. Probab.* **13** 79 arXiv:0706.3334 [math.PR]

[12] Bouttier J and Guitter E, *Statistics of geodesics in large quadrangulations*, 2008 *J. Phys. A: Math. Theor.* **41** 145001 arXiv:0712.2160 [math-ph]

[13] Miermont G, *Tessellations of random maps of arbitrary genus*, 2007 arXiv:0712.3688 [math.PR]

[14] Le Gall J-F, *Geodesics in large planar maps and in the Brownian map*, 2008 arXiv:0804.3012 [math.PR]

[15] Bouttier J and Guitter E, *The three-point function of planar quadrangulations*, 2008 *J. Stat. Mech.* P07020 arXiv:0805.2355 [math-ph]

[16] Aoki H, Kawai H, Nishimura J and Tsuchiya A, *Operator product expansion in two-dimensional quantum gravity*, 1996 *Nucl. Phys.* B **474** 512 [arXiv:hep-th/9511117]

[17] Marcus M and Schaeffer G, *Une bijection simple pour les cartes orientables*, 2001 available at http://www.lix.polytechnique.fr/Labo/Gilles.Schaeffer/Biblio/
See also Schaeffer G, *Conjugaison d'arbres et cartes combinatoires aléatoires*, 1998 *PhD Thesis* Université Bordeaux I
Chapuy G, Marcus M and Schaeffer G, *A bijection for rooted maps on orientable surfaces*, 2007 arXiv:0712.3649 [math.CO]

[18] Cori R and Vauquelin B, *Planar maps are well labeled trees*, 1981 *Can. J. Math.* **33** 1023

[19] Delmas J-F, *Computation of moments for the length of the one-dimensional ISE support*, 2003 *Electron. J. Probab.* **8** 1

[20] Bousquet-Mélou M, *Limit laws for embedded trees. Applications to the integrated superBrownian excursion*, 2006 *Random Struct. Algorithms* **29** 475 [arXiv:math.CO/0501266]

[21] Bouttier J, *Physique statistique des surfaces aléatoires et combinatoire bijective des cartes planaires*, 2005 *PhD Thesis*

[22] Jain S and Mathur S, *World-sheet geometry and baby universes in 2D quantum gravity*, 1992 *Phys. Lett.* B **286** 239 [arXiv:hep-th/9204017]

[23] Banderier C, Flajolet P, Schaeffer G and Soria M, *Random maps, coalescing saddles, singularity analysis, and airy phenomena*, 2001 *Random Struct. Algorithms* **19** 194

[24] Duplantier B and Sheffield S, *Liouville Quantum Gravity and KPZ*, 2008 arXiv:0808.1560 [math.PR]

[25] David F and Bauer M, *Another derivation of the geometrical KPZ relations*, 2008 arXiv:0810.2858 [math-ph]

[26] Boulatov D and Kazakov V, *The Ising model on a random planar lattice: the structure of the phase transition and the exact critical exponents*, 1987 *Phys. Lett.* B **186** 379

[27] Bousquet-Mélou M and Schaeffer G, *The degree distribution in bipartite planar maps: application to the Ising model*, 2002 arXiv:math.CO/0211070

[28] Bouttier J, Di Francesco P and Guitter E, *Combinatorics of hard particles on planar graphs*, 2003 *Nucl. Phys.* B **655** 313 [arXiv:cond-mat/0211168]

[29] Bouttier J, Di Francesco P and Guitter E, *Combinatorics of bicubic maps with hard particles*, 2005 *J. Phys. A: Math. Gen.* **38** 4529 [arXiv:math.CO/0501344]

[30] Bouttier J, Di Francesco P and Guitter E, *Planar maps as labeled mobiles*, 2004 *Electron. J. Combin.* **11** R69 [arXiv:math.CO/0405099]

[31] Bouttier J, Di Francesco P and Guitter E, *Blocked edges on Eulerian maps and mobiles: application to spanning trees, hard particles and the Ising model*, 2007 *J. Phys. A: Math. Theor.* **40** 7411 [arXiv:math.CO/0702097]

J. Stat. Mech. (2009) P03001